Radiation-induced acid ceramidase confers prostate cancer resistance and tumor relapse

Joseph C. Cheng,[1] Aiping Bai,[2] Thomas H. Beckham,[1] S. Tucker Marrison,[1] Caroline L. Yount,[3] Katherine Young,[3] Ping Lu,[1] Anne M. Bartlett,[4] Bill X. Wu,[2] Barry J. Keane,[1] Kent E. Armeson,[5] David T. Marshall,[3] Thomas E. Keane,[6] Michael T. Smith,[4] E. Ellen Jones,[7] Richard R. Drake Jr.,[7] Alicja Bielawska,[2] James S. Norris,[1] and Xiang Liu[1]

[1]Department of Microbiology and Immunology, [2]Department of Biochemistry, [3]Department of Radiation Oncology, [4]Department of Pathology and Laboratory Medicine, [5]Department of Biostatistics and Epidemiology, [6]Department of Urology, and [7]Department of Pharmacology, Medical University of South Carolina, Charleston, South Carolina, USA.

Escape of prostate cancer (PCa) cells from ionizing radiation–induced (IR-induced) killing leads to disease progression and cancer relapse. The influence of sphingolipids, such as ceramide and its metabolite sphingosine 1-phosphate, on signal transduction pathways under cell stress is important to survival adaptation responses. In this study, we demonstrate that ceramide-deacylating enzyme acid ceramidase (AC) was preferentially upregulated in irradiated PCa cells. Radiation-induced AC gene transactivation by activator protein 1 (AP-1) binding on the proximal promoter was sensitive to inhibition of de novo ceramide biosynthesis, as demonstrated by promoter reporter and ChIP-qPCR analyses. Our data indicate that a protective feedback mechanism mitigates the apoptotic effect of IR-induced ceramide generation. We found that deregulation of c-Jun induced marked radiosensitization in vivo and in vitro, which was rescued by ectopic AC overexpression. AC overexpression in PCa clonogens that survived a fractionated 80-Gy IR course was associated with increased radioresistance and proliferation, suggesting a role for AC in radiotherapy failure and relapse. Immunohistochemical analysis of human PCa tissues revealed higher levels of AC after radiotherapy failure than those in therapy-naive PCa, prostatic intraepithelial neoplasia, or benign tissues. Addition of an AC inhibitor to an animal model of xenograft irradiation produced radiosensitization and prevention of relapse. These data indicate that AC is a potentially tractable target for adjuvant radiotherapy.

Introduction

Over the past decade, with the advent of advanced CT-based treatment, planning intensity modulated radiotherapy has gained ascendency over other radiation approaches for primary prostate cancer (PCa) treatment (1–4). For patients who have not undergone prostatectomy, radiation therapy involves a treatment course of greater than 70 Gy usually administered in daily fractions of 1.8 to 2 Gy over a 7- to 9-week period. A recent study found distant (≤10 years) biochemical control in high-risk patients to be as low as 52.7%, with overall local and distant recurrence rates among all risk groups at 5.1% and 8.6%, respectively (4), similar to previous data (5–10). Although the delivery of higher doses of ionizing radiation (IR) improves local control (11–13), conventional techniques of dose escalation come up against dose-limiting toxicities to noncancerous tissues (4, 14–16). Therefore, for purposes of better control of such patients, the molecular mechanisms underlying PCa cell radioresistance and methods to interdict such resistance must be understood in order to maximize the curative potential of radiation therapy.

Bioactive sphingolipids, particularly ceramide, sphingosine, and sphingosine 1-phosphate (S1P), known as the "ceramide-S1P rheostat" (17), are recognized as critical signaling initiators that regulate cell survival, death, proliferation, and inflammation. As appreciation grows for the role of sphingolipids in vital biological processes (18, 19), efforts to target their expression for therapeutic benefit have also gained traction (20–22). In the context of radiation therapy, characterization of IR-induced sphingolipid processing in programmed cell death has demonstrated ceramide generation through both membrane-associated sphingomyelin hydrolysis and genotoxicity-associated de novo mechanisms (23–27). Stress-activated protein kinase (28) and Bcl-2 family–induced mitochondrial depolarization pathways (25) are proximal downstream targets of ceramide accumulation after IR. However, radioresistance may be elicited by either defects in ceramide generation (29–32) or rapid turnover of ceramide into S1P (33–35). Rescue of the apoptotic phenotype by restoring ceramide accumulation or limiting S1P signaling is currently being studied both at the basic science and clinical levels (36–38).

Irradiation of tumors is a potent death-inducing stimulus that rapidly evolving cancer cells frequently escape by virtue of previously existing mutations in death pathways or by responding to the insult reactively to activate survival pathways. While the characterization of aberrant, cancer-associated gene expression in tissues obtained for diagnosis versus noncancerous tissues is a prominent arena of research (39), the response of tumors to therapy also represents a critical avenue of investigation (22). Work by this group and others has demonstrated that the ceramide-metabolizing enzyme, acid ceramidase (AC), can play an important role in resistance to anticancer therapies (40–47), including IR (26, 36, 48, 49). In this report, we evaluated transcriptional activation of AC in PCa cells treated with radiation. We found that the AC gene (N-acylsphingosine amidohydrolase [*ASAH1*]) promoter is a target of ceramide-dependent c-Jun/activator protein 1 (c-Jun/AP-1) binding, suggestive of a

Authorship note: James S. Norris and Xiang Liu are co–senior authors.

Conflict of interest: Alicja Bielawska and James S. Norris hold stock in SphingoGene Inc., which is trying to develop LCL521 as a clinical drug for treating cancer.

Citation for this article: *J Clin Invest.* 2013;123(10):4344–4358. doi:10.1172/JCI64791.

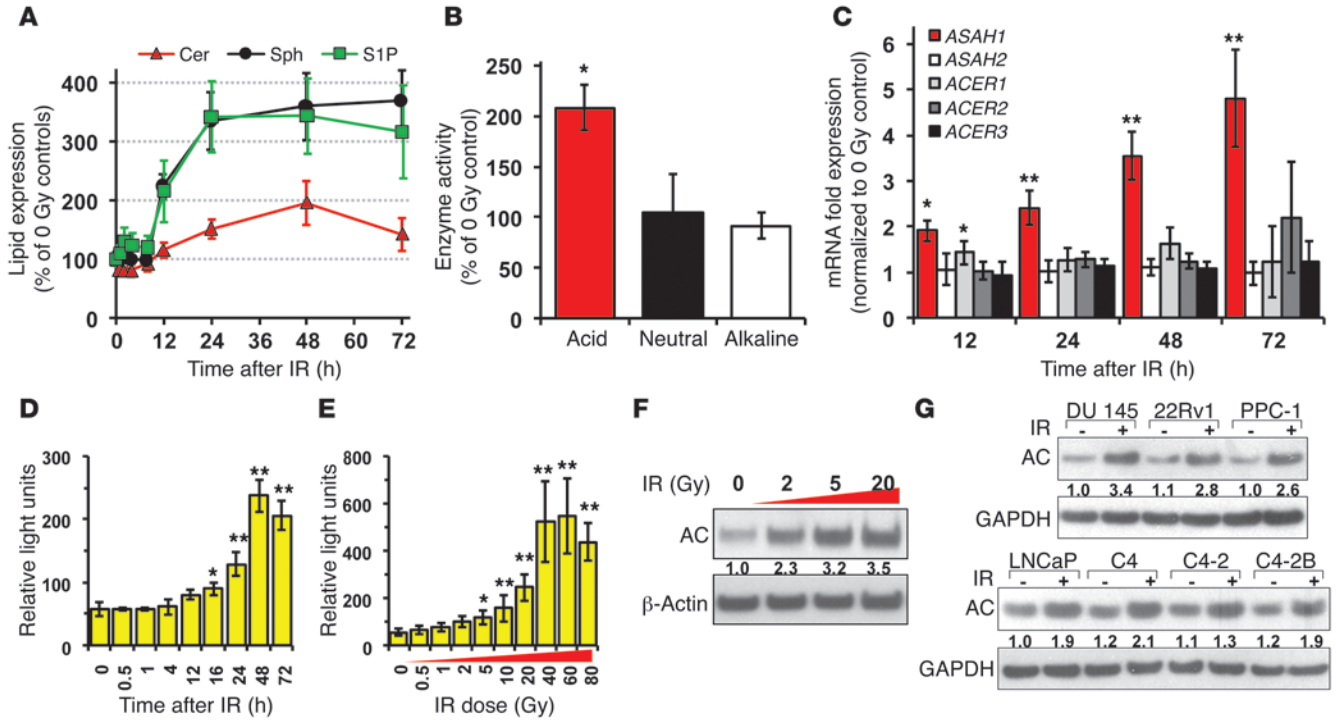

Figure 1

IR selectively upregulates AC in prostate cancer cells. (**A**) Sphingolipid content of PPC-1 cells analyzed between 15 minutes and 72 hours after γ irradiation (5 Gy). Intracellular levels of total ceramide (Cer), sphingosine (Sph), and S1P are shown relative to those of nonirradiated controls. (**B**) Enzyme activity of PPC-1 whole cell lysates collected 24 hours after IR (5 Gy) at pH optima for acid, neutral, or alkaline ceramidase isozymes compared with that of nonirradiated controls ($n = 4$). (**C**) mRNA expression of the AC gene (*ASAH1*), neutral ceramidase (*ASAH2*), and alkaline ceramidases (*ACER1*, *ACER2*, and *ACER3*) in PPC-1 cells assessed by RT-qPCR up to 72 hours after IR (5 Gy). Genes of interest are normalized to *RPS15* and shown relative to nonirradiated controls. Luciferase activity of PPC-1 cells expressing pLVX-*ASAH1*-Luc promoter reporter was assessed at (**D**) various times after IR (5 Gy) or (**E**) at various radiation doses 24 hours after IR. (**F**) PPC-1 cells and (**G**) other cell lines derived from prostate adenocarcinomas were assessed 48 hours after IR for protein expression by Western blot. Mean densitometry of normalized AC expression is shown below each band. $^*P < 0.05$, $^{**}P < 0.01$.

transactivation feedback trigger to reverse the proapoptotic effects of IR-induced ceramide accumulation. Fractioned irradiation of PCa cells to a cumulative dose of 80 Gy induced and/or selected for PCa cell clonogens, of which 90% demonstrated constitutive AC overexpression that correlated with increased proliferation and radioresistance. AC expression was found to be upregulated in human prostate adenocarcinomas compared with that in noncancer tissues and to an even greater extent in tissues from patients who failed radiation therapy. Finally, we found that AC can be specifically targeted in vivo, in combination with IR, to achieve a durable cure in mouse xenograft models. Taken together, these results indicate that sphingolipid metabolism, particularly ceramide processing by AC, is a functionally important and druggable target to improve responses to radiation therapy.

Results

IR induces selective upregulation of AC in cancer cells. In order to determine whether IR exposure induces a change in PCa cell sphingolipid expression, we assessed ceramide, sphingosine, and S1P levels in the hormone-refractory PPC-1 cell line treated with 5-Gy IR versus mock irradiation. As shown in Figure 1A, cellular sphingolipid levels were not significantly altered between 15 minutes and 8 hours after irradiation (specific ceramide species are shown in Supplemental Figure 1A; supplemental material available online with this article; doi:10.1172/JCI64791DS1). However, sphingolipid levels were elevated by 12 hours after IR and achieved maximum expression between 24 and 72 hours. Specifically, total ceramide content increased between 40% to 100%, whereas the products of ceramide catabolism, sphingosine and S1P, demonstrated 200%- to 270%-increased expression. Irradiation was also associated with a 3-fold increase of S1P detected in the cell culture supernatants (Supplemental Figure 1B), indicating that IR exposure elicited a marked shift of sphingolipid content toward the soluble products of ceramide metabolism.

Given that several ceramidase isozymes catalyze the hydrolysis of ceramide to sphingosine and free fatty acid, we sought to determine which enzymes were induced by IR based on their pH optima. Homogenates of 5 Gy– and mock-irradiated PPC-1 cells were tested for ceramidase activity at pH 4.5, 7.5, or 9.5 (Figure 1B). Two-fold enhancement of enzyme activity was detected in irradiated cells at acidic pH, while activity at neutral and alkaline pH remained unchanged, suggesting that the lysosomal isozyme, AC, may be largely responsible for ceramide-to-sphingosine processing under irradiative stress. Marked and sustained increase of mRNA expression of the AC gene, *ASAH1*, but not neutral ceramidase, *ASAH2*, or alkaline ceramidases, *ACER1*, *ACER2*, and *ACER3*, was detected in PPC-1 cells through 72 hours after IR exposure (Figure 1C). Firefly luciferase–based activity reporter assay demonstrated

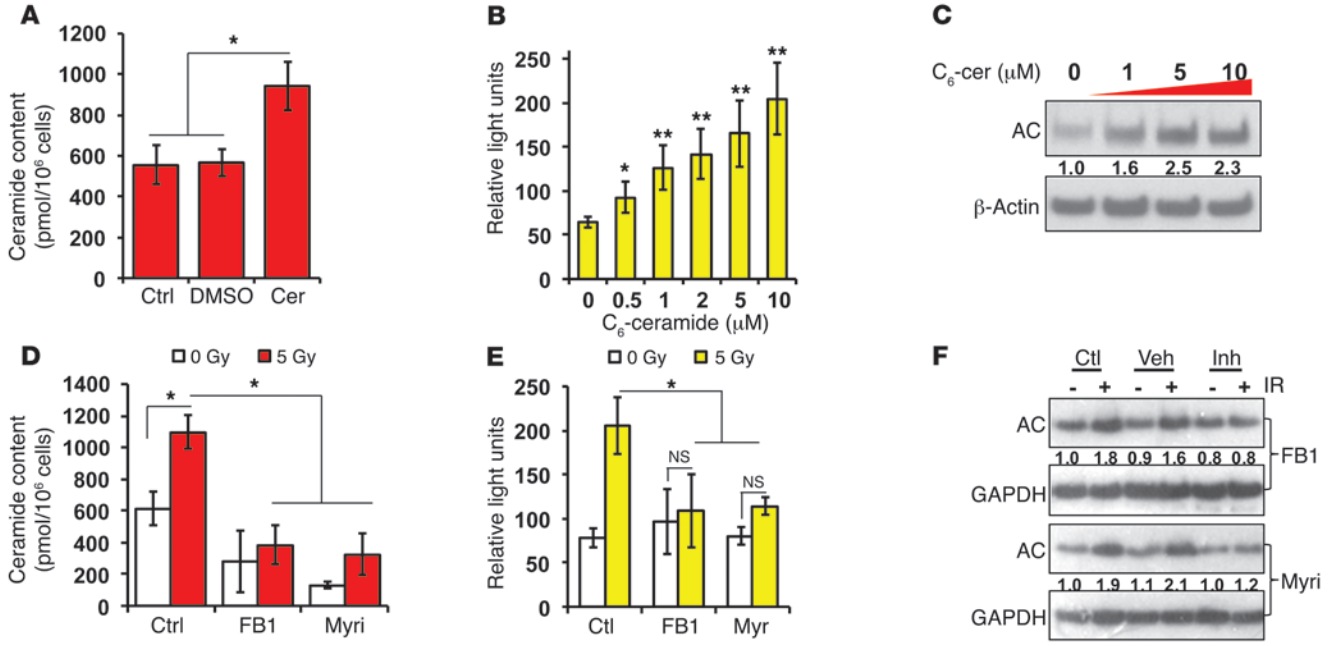

Figure 2

IR-stimulated ceramide induces AC gene expression. PPC-1 cells were treated with C_6-ceramide (5 μM) or DMSO (vehicle control) for 12 hours and analyzed for (**A**) endogenous ceramide content and (**B**) *ASAH1* promoter reporter activity. (**C**) Western blot of cell lysates collected after 24 hours of C_6-ceramide treatment. PPC-1 cells pretreated with ceramide pathway inhibitors FB1 (25 μM), myriocin (Myri; 100 nM), or DMSO control for 4 hours were subjected to γ irradiation (5 Gy), and 24 hours after IR, cells were analyzed for (**D**) endogenous ceramide content, (**E**) *ASAH1* promoter reporter activity, and (**F**) AC protein expression. Veh, vehicle control; Inh, inhibitor. Mean densitometry of normalized AC expression is shown below each band. $^*P < 0.05$, $^{**}P < 0.01$.

dose-dependent transcription activation beginning at 12 hours after IR (Figure 1, D and E), which corresponded with AC protein upregulation (Figure 1F). IR also upregulated AC in the prostate adenocarcinoma cell lines DU 145, CWR-22Rv1, and LNCaP (Figure 1G). Interestingly, we have not evinced similar upregulation of ceramide content or AC expression by IR exposure to noncancer prostate cell lines PWR-1E (immortalized epithelium), WPMY-1 (immortalized stroma), or PrEC (primary epithelium), as shown in Supplemental Figure 8. Yet, cell lines derived from various other adenocarcinomas or squamous cell carcinomas also demonstrated AC protein overexpression upon γ irradiation (Supplemental Figure 1C). Taken together, these data suggest that many cancers respond to IR by upregulating AC, likely as a response to mitigate the deleterious effects of stress-induced ceramide accumulation.

AP-1 regulates ceramide-dependent AC gene transactivation by IR. Based on the above results, we hypothesized that IR-induced ceramide generation constitutes a feedback stimulus that induces AC expression. To test this, we first assessed PPC-1 cell expression of AC under direct ceramide modulation. Exogenous delivery of C_6-ceramide, an artificial short acyl-chain ceramide, increased intracellular levels of natural-length ceramides (Figure 2A) and concomitantly enhanced both reporter activity of the *ASAH1* promoter (Figure 2B) and expression of AC protein (Figure 2C). Since ceramide profiling indicated that treatment with either IR (50) or short-chain ceramide stimulates a relative increase of C_{16}-ceramide among all species (Supplemental Figure 2A), we ectopically expressed an adenoviral transgene encoding ceramide synthase-6 (CerS6) to preferentially synthesize C_{16}-ceramide. Similar to exogenous C_6-ceramide treatment, endogenous ceramide generation by CerS6 significantly enhanced cellular ceramide content (Supplemental Figure 2, A and B), *ASAH1* promoter activity (Supplemental Figure 2C), and AC protein expression (Supplemental Figure 2D). These results demonstrated that exogenously or ectopically upregulated ceramide stimulated AC gene expression.

In order to evaluate native mechanisms of ceramide biosynthesis in PCa cell response to IR, we administered inhibitors of ceramide generation prior to γ irradiation. Pretreatment of PPC-1 cells with either an inhibitor of ceramide synthase, fumonisin B_1 (FB1) (51), or an inhibitor of serine palmitoyltransferase, myriocin (52), resulted in both suppression of baseline intracellular ceramide levels and abrogation of IR-induced ceramide (Figure 2D). In addition, use of either inhibitor abrogated IR-induced *ASAH1* reporter activity (Figure 2E) and AC protein upregulation (Figure 2F). Inhibition of ceramide generation by acid sphingomyelinase, either through desipramine (53) administration (Supplemental Figure 3A) or by RNAi transfection (Supplemental Figure 3B), did not interrupt IR-induced AC upregulation. Altogether, these results implicated the myriocin- and FB1-sensitive pathways of ceramide generation as the primary feedback cues for IR-induced AC upregulation, whereas ceramide generation through sphingomyelin metabolism was not a significant contribution. Furthermore, neither *ASAH1* reporter activity nor AC protein expression were altered under conditions of exogenous S1P delivery (data not shown) or sphingosine kinase inhibitor (SKI-II; 1.0 μM) administration prior to γ irradiation (Supplemental Figure 3, C–E), indicating that IR-induced AC transactivation is regulated at the level of ceramide accumulation rather than downstream metabolism into a S1P-dependent feed-forward mechanism.

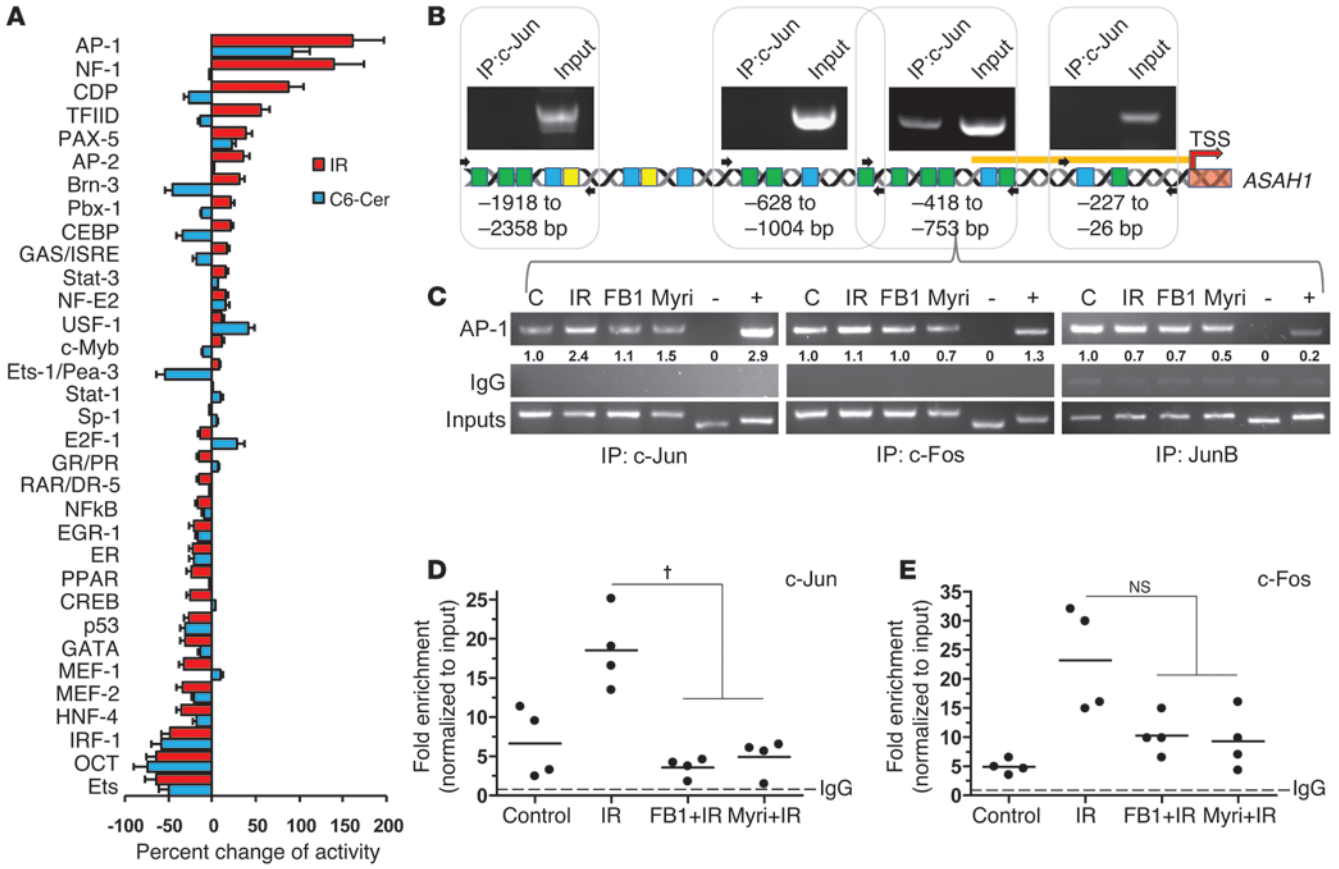

Figure 3

ASAH1 is a ceramide-sensitive target of IR-induced AP-1 binding. (**A**) Transcription factor activity assay of PPC-1 cell nuclear extracts collected after irradiation (5 Gy, 24 hours) or C_6-ceramide (2 μM, 12 hours), as compared with untreated control. (**B**) γ-Irradiated PPC-1 cells (5 Gy, 24 hours) were subjected to ChIP targeting c-Jun–bound segments of the *ASAH1* promoter with the highest concentration of putative AP-1 consensus binding sequences. Schematic of *ASAH1* proximal promoter is annotated with binding sequences predicted by TESS (yellow) or TFBIND (blue) analyses or both (green). The orange line denotes the length of the –496-bp luciferase reporter used in Supplemental Figure 5. Arrows denote the positions of forward and reverse ChIP primers. (**C**) ChIP for c-Jun, c-Fos, or JunB binding to –753/–418 *ASAH1* promoter fragment. PPC-1 cells were pretreated with ceramide pathway inhibitors, FB1 (25 μM) or myriocin (0.1 μM, 4 hours), irradiated (5 Gy, 24 hours), and evaluated for c-Jun binding to the *ASAH1* promoter. An intronic *ASAH1* sequence with no AP-1 consensus binding site was used as a negative control (–); a –243/–3 *MMP1* promoter sequence was used as a positive control (+). Mean densitometry of AP1 amplicons normalized to input controls is shown. C, nonirradiated control. These eluates were quantitated by ChIP-qPCR analysis for (**D**) c-Jun or (**E**) c-Fos binding to the *ASAH1* promoter. Results are expressed as fold of expression normalized to IgG pull-down controls ($n = 4$). †$P < 0.05$, Kruskal-Wallis test, Dunn post-hoc analysis.

We next sought to investigate whether this mechanism of AC induction was regulated at the transcriptional level, as the *ASAH1* promoter reporter indicated. We subjected nuclear fractions of PPC-1 cells treated with either IR (5 Gy, 24 hours) or C_6-ceramide (2 μM, 12 hours) to a DNA-protein binding assay, which demonstrated increased AP-1 activity under either condition (Figure 3A). Targeting the prototypical Jun/Fos members of the AP-1 family with pooled- or single-sequence RNAi transfection implicated c-Jun, and possible c-Fos, involvement in AC gene expression under both basal conditions (Supplemental Figure 4 and Supplemental Figure 5, A and B) and IR induction (Supplemental Figure 5, A and B).

In silico identification of AP-1 consensus binding sequences in the *ASAH1* promoter revealed 4 high-density regions of putative binding sites (Figure 3B), which became the targets for interrogation by ChIP. ChIP assay confirmed c-Jun/AP-1 binding within the –628/–418–bp sequence upstream of *ASAH1* start codon (Figure 3B). Evaluation of a series of truncated *ASAH1* promoter-LUC reporters (54, 55), demonstrated regulatory *cis*-element(s) involved in IR-mediated AC gene expression within the –496-bp promoter region (Supplemental Figure 5C). TCA→TTG mutations to nullify 3 AP-1 consensus binding sequences within the –496-bp region abrogated IR-induced *ASAH1* promoter activation at the site –475/–468 bp, with possible combinatorial involvement of the nearby –494/–486–bp binding site (Supplemental Figure 5D).

Finally, ChIP-qPCR analyses of irradiated PPC-1 cells demonstrated enrichment of c-Jun binding to the *ASAH1* promoter (Figure 3, C and D). Moreover, this phenomenon occurred in a myriocin- and FB1-sensitive manner. c-Fos binding on the *ASAH1* promoter demonstrated a similar trend of upregulation upon IR exposure, which was countered by FB1 and myriocin pretreatment, although results were shy of significance (Figure 3, C and E). Interestingly, exogenous C_6-ceramide treatment recapitulated induction of c-Jun and c-Fos binding, which was inhibited by FB1 pretreatment but not myriocin pretreatment

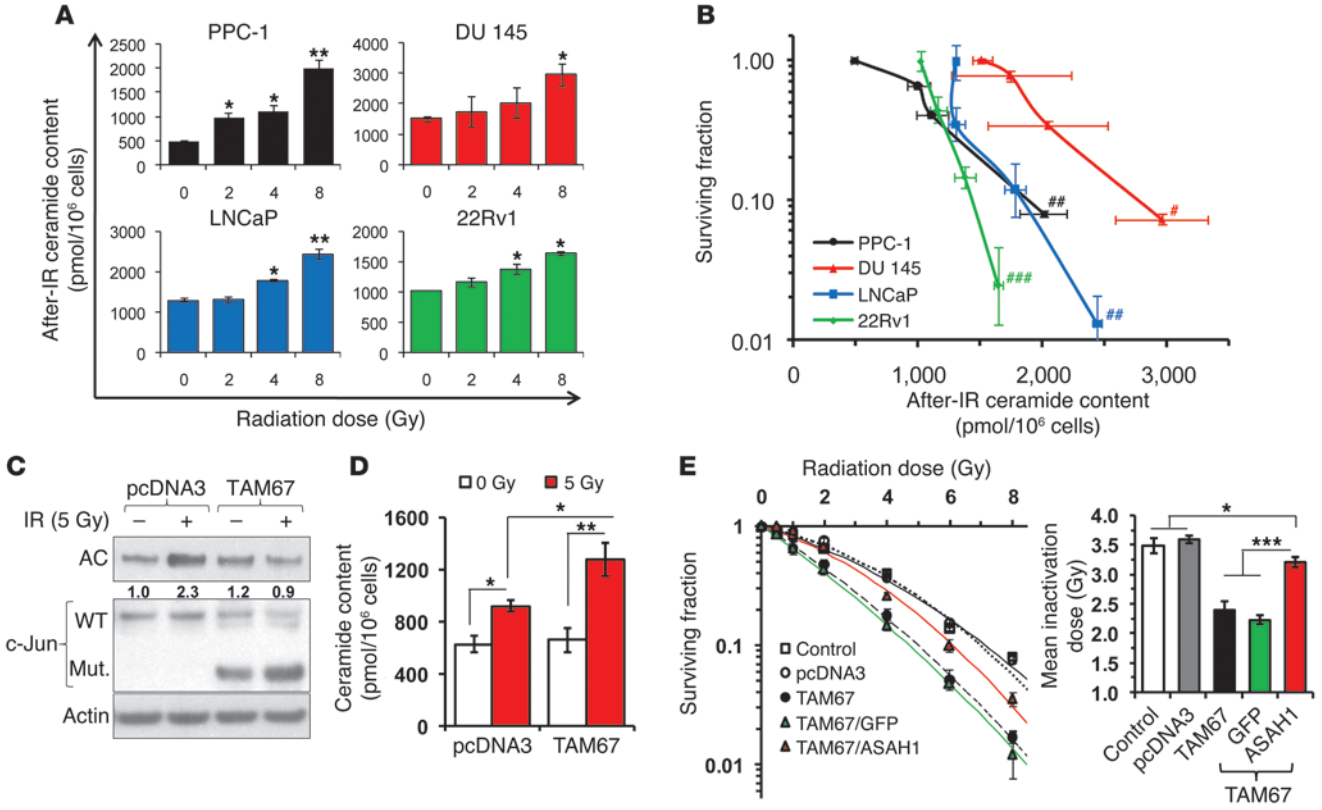

Figure 4

c-Jun–regulated AC mediates PCa cell radioresistance. (**A**) Intracellular ceramide content of PCa cell lines 48 hours after IR (5 Gy). (**B**) Clonogenic survival of PCa cell lines plotted against IR-stimulated ceramide content shown in **A**. (**C**) Protein expression and (**D**) ceramide content in γ-irradiated (5 Gy, 24 hours) PPC-1 cells stably expressing the c-Jun dominant-negative transactivation mutant TAM67 or the pcDNA3 empty vector control. Mean densitometry of normalized AC expression is shown. (**E**) Radiation sensitivity of PPC-1 cells expressing the dominant-negative c-Jun mutant, TAM67 (versus parental or pcDNA3 controls), with or without ectopic overexpression of AC based on adenoviral Ad*ASAH1*-GFP (10 MOI; versus AdGFP control) transduction ($n = 5$). Results are shown as geometric mean ± SEM (left panel) and fitted to the linear-quadratic model to quantify mean inactivation dose (right panel). $^{*}P < 0.05$, $^{**}P < 0.01$, $^{***}P < 0.001$, 1-way ANOVA and Tukey-Kramer post-hoc analysis. $^{\#}P < 0.05$, $^{\#\#}P < 0.01$, $^{\#\#\#}P < 0.001$, Spearman rank correlation.

(Supplemental Figure 6, C and D). Although JunB binding to the *ASAH1* promoter was confirmed by ChIP assay (Figure 3C and Supplemental Figure 6C), it failed to respond to stimulation with IR (Figure 3C) or exogenous ceramide (Supplemental Figure 6C). Taken together, these results confirmed that c-Jun activity is a predominant factor in the feedback mechanism by which IR-induced ceramide causes *ASAH1* transcription.

c-Jun–mediated AC promotes PCa radiation resistance and relapse in vitro and in vivo. The functional consequences of IR-induced c-Jun regulating AC was of importance to investigate. IR dose corresponded to increased ceramide expression levels in several PCa cell lines (Figure 4A). Moreover, ceramide levels after IR correlated with clonogenic cell death in the case of each cell line tested (Figure 4B). PPC-1 cells pretreated with inhibitors of ceramide-generating enzymes, FB1, or myriocin were less susceptible to IR-induced caspase-3/7 activation (Supplemental Figure 3F), indicating involvement of the de novo ceramide generation pathway in cell killing. We found that inhibition of AC by RNAi contributes, in large part, to this clonogenic collapse by increasing PCa susceptibility to IR-induced caspase activation, annexin V expression, and apoptosis (Supplemental Figure 10, A–C, respectively). In this study, IR-induced necrosis (Supplemental Figure 10D) was not found to play a significant role in the functional outcome of IR treatment on PCa cells. Importantly, as described below, the rescue of AC overexpression upon IR challenge confirmed its cell survival role in PCa.

In order to assess the contribution of c-Jun–regulated AC to the response of PCa cells to IR, we stably expressed a dominant-negative transactivation mutant of c-Jun, TAM67 (56–58), in PPC-1 cells. Irradiation of these TAM67-expressing cells did not upregulate AC (Figure 4C) and induced even more ceramide accumulation (Figure 4D) than control (pcDNA3 empty vector). AC overexpression stimulated by C_6-ceramide administration was similarly attenuated in TAM67-expressing PPC-1 cells (Supplemental Figure 7A). Although TAM67 expression did not change the proliferation rate of PPC-1 cells under basal growth conditions (Supplemental Figure 7B), it did enhance IR-induced clonogenic cell killing compared with empty vector expression or nontransfected parental control (Figure 4E). While this observation implicated a vital role for c-Jun in the cell response to IR, we interrogated downstream involvement of AC by rescuing this phenotype with transduction of Ad*ASAH1* overexpression plasmid (Supplemental Figure 7C). PPC-1–TAM67 cells transduced with Ad*ASAH1*-GFP (10 MOI) prior to irradiation demonstrated significant reversal

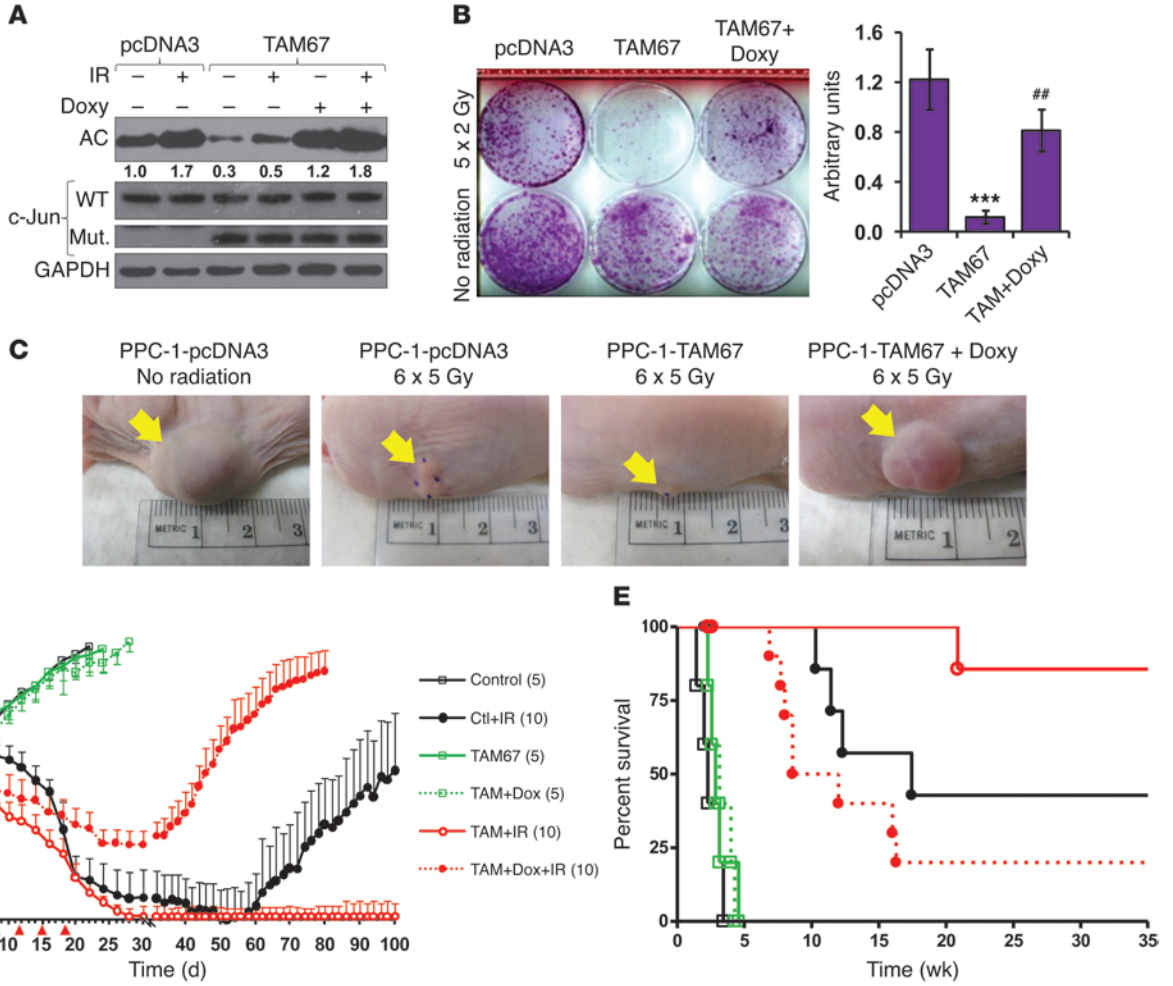

Figure 5

c-Jun–regulated AC mediates PCa cell radioresistance. (**A**) Protein expression in PPC-1 cells expressing a doxycycline-inducible AC expression vector, tetO*ASAH1*, incubated with doxycycline (25 ng/ml) and/or after IR (5 Gy) for 48 hours. Mean densitometry of normalized AC expression is shown. (**B**) PPC-1–TAM67–tetO*ASAH1* cells with or without doxycycline incubation (25 ng/ml) were subjected to daily 2-Gy IR fractions for a cumulative dose of 10 Gy (compared with PPC-1–pcDNA3–tetO*ASAH1* cells). $^{\#\#}P < 0.01$ compared with TAM67 plus IR; $^{***}P < 0.001$ compared with pcDNA3 plus IR. (**C**) Subcutaneous xenografts grown on the flanks of athymic *nu/nu* mice were subjected to 5-Gy fractions of focal γ irradiation (red triangles in **D**) to a cumulative dose of 30 Gy. Xenografts are depicted at the end of radiation therapy (day 22–24). (**D**) Xenograft volumes and (**E**) overall survival were monitored; *n* per group is noted parenthetically.

of the TAM67 radiosensitization phenotype (Figure 4E). These results confirm that interference of IR-induced AC transactivation renders PCa cells susceptible to the proapoptotic influence of ceramide accumulation in vitro.

A study of PPC-1–derived xenografts in athymic *nu/nu* mice elucidated the effects of c-Jun/AP-1 deregulation and ectopic AC reconstitution on PCa resistance to and relapses following radiation therapy (Figure 5, C–E). PPC-1–pcDNA3 or PPC-1–TAM67 cells were inoculated into the flanks of nude mice to establish subcutaneous xenografts (128 ± 3 mm^3) that were subjected to a hypofractionated schedule of focal irradiation (6 × 5 Gy). There was no significant difference in the growth rate of mock-irradiated pcDNA3 or TAM67 xenografts. However, TAM67 xenografts demonstrated immediate response to radiation therapy, and, upon completion of radiotherapy by day 22, TAM67 xenograft volumes were diminished 81% versus 67% diminution of pcDNA xenografts ($P = 0.012$). pcDNA3 xenografts demonstrated relapse/regrowth within 8 weeks of therapy initiation, whereas 30 Gy total IR was sufficient to produce cure of 80% of TAM67 xenografts through 35 weeks of evaluation.

In addition to the pcDNA3-TAM67 construct, these PPC-1–derived xenografts also harbored a pcDNA5-tetO*ASAH1* construct (59) that restored AC overexpression in a doxycycline-responsive manner (Figure 5A). Similar to our observation from adenoviral-based *ASAH1* transgene expression, doxycycline induction of AC significantly increased radiation resistance of PPC-1–TAM67 cells in vitro (Figure 5B). In the xenograft model, addition of doxycycline to the drinking water (250 mg/l) of mice bearing TAM67-tetO*ASAH1* xenografts resulted in increased radiation resistance of the xenografts: upon completion of radiotherapy by day 22, there was no significant reduction of volumes since the beginning of treatment (Figure 5, C and D). Furthermore, xenograft regrowth occurred 3 weeks sooner and overall survival of mice was diminished compared with that of irradiated PPC-1–pcDNA3 xenografts

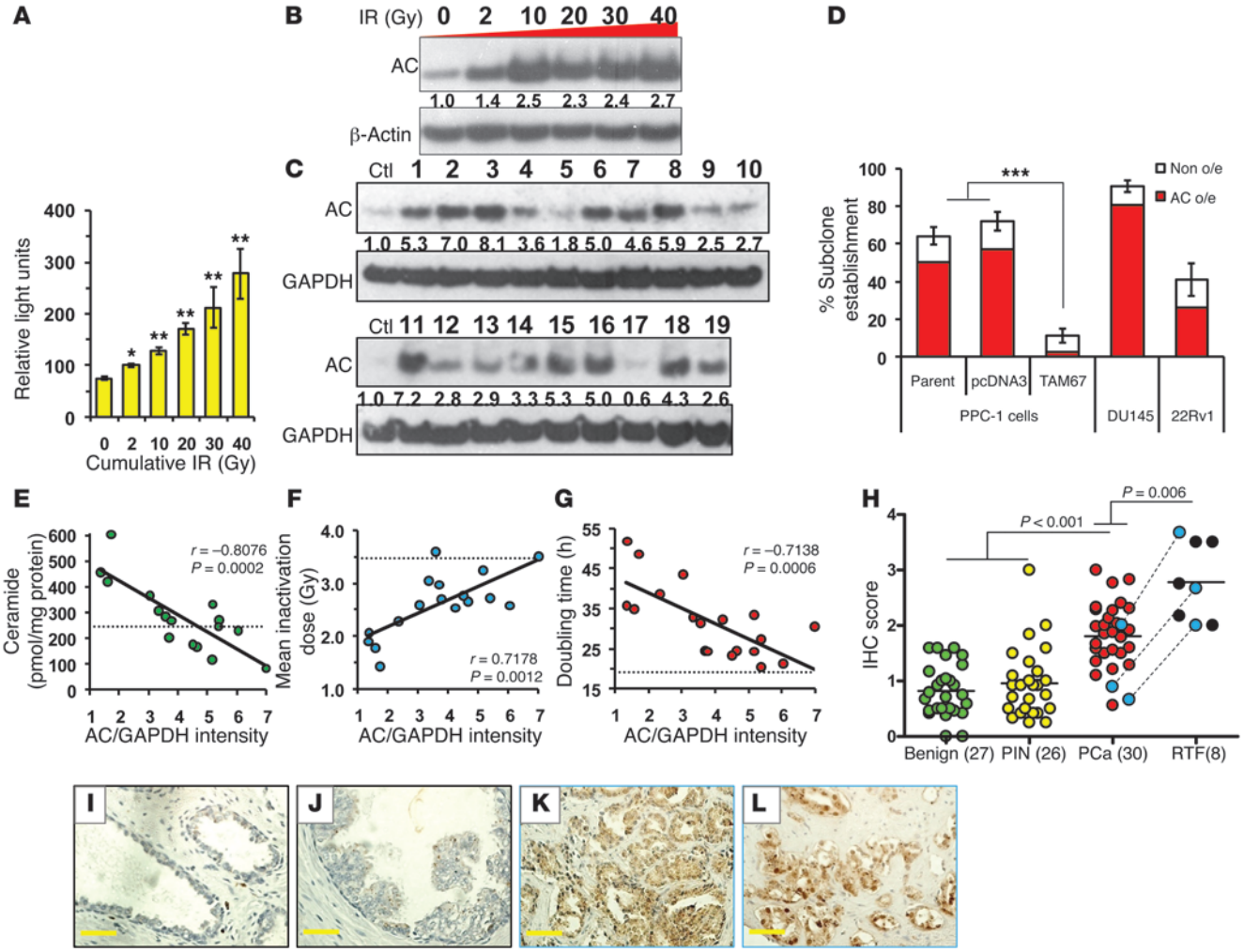

Figure 6

Recurrent PCa after radiation therapy overexpresses AC. PPC-1 cells were subjected to fractionated radiotherapy (40 × 2 Gy) and evaluated (**A**) for *ASAH1* promoter reporter activity (luciferase assay) and (**B**) for AC protein expression (representative immunoblot) versus nonirradiated control cells. (**C**) PPC-1 cell subclones grown after a cumulative IR dose of 80 Gy were assessed for AC protein expression by Western blot. (**B** and **C**) Mean densitometry of normalized AC expression is shown. (**D**) The frequencies of clonal repopulation from single-cell cultures of 80 Gy–surviving PCa cells are shown as the combinations of subclones overexpressing (o/e) AC (red) and those not overexpressing AC (white), as determined by immunoblot versus nonirradiated control cells. AC expression in PPC-1 subclones shown in **D** was quantified based on AC/GAPDH band densitometry and (**E**) was assessed for Pearson correlation to cellular ceramide content; (**F**) radiation resistance, as determined by mean inactivation dose from clonogenic survival assays; and (**G**) doubling rate. Dotted lines indicate mean ceramide content, inactivation dose, and doubling rate, respectively, of IR-naive control PPC-1 cells. (**H**) AC expression in prostate biopsies of benign, PIN, therapy-naive adenocarcinoma, and biochemical recurrence/failure after definitive radiotherapy (RTF). Representative images of AC expression (brown) against hematoxylin counterstain (blue) are shown for (**I**) benign, (**J**) PIN, (**K**) therapy-naive adenocarcinoma, and (**L**) RTF tissues. Scale bar: 50 μm. Representative images and immunohistochemistry scores of patient-matched tissues are depicted in **K** and **L** and by blue circles connected by dotted lines in **H**. $^{*}P < 0.05$, $^{**}P < 0.01$, $^{***}P < 0.001$.

(Figure 5, D and E). Taken together, these results demonstrate a significant role for c-Jun–mediated AC upregulation in the survival response of PCa cells during radiation therapy.

Recurrent PCa after radiation therapy overexpresses AC. To examine the association between AC and PCa cell regrowth/relapse after radiotherapy, we administered to PPC-1 cells a regimen of daily 2-Gy fractions to a cumulative IR dose of 80 Gy in vitro. Throughout the course of this experiment, irradiated cells demonstrated enhanced *ASAH1* promoter activity (Figure 6A) and AC protein expression (Figure 6B) concomitant with IR exposure. Despite achieving prototypical logarithmic cell killing, we recovered surviving adherent cells at the culmination of radiation treatment and seeded them in single-cell cultures to evaluate clonogenicity. 41%–91% of surviving cancer cells (from the cell lines PPC-1, DU 145, and 22Rv1) maintained clonogenicity after 80 Gy. PPC-1–pcDNA3 cells reconstituted clonal populations at a frequency of 72%, similar to PPC-1 parental cells, whereas only 11% of IR-surviving PPC-1–TAM67 cells reestablished colonies (Figure 6D). Moreover, a majority of the subclones grown from IR-surviving PPC-1, DU 145, and 22Rv1 PCa cell lines continued to overexpress

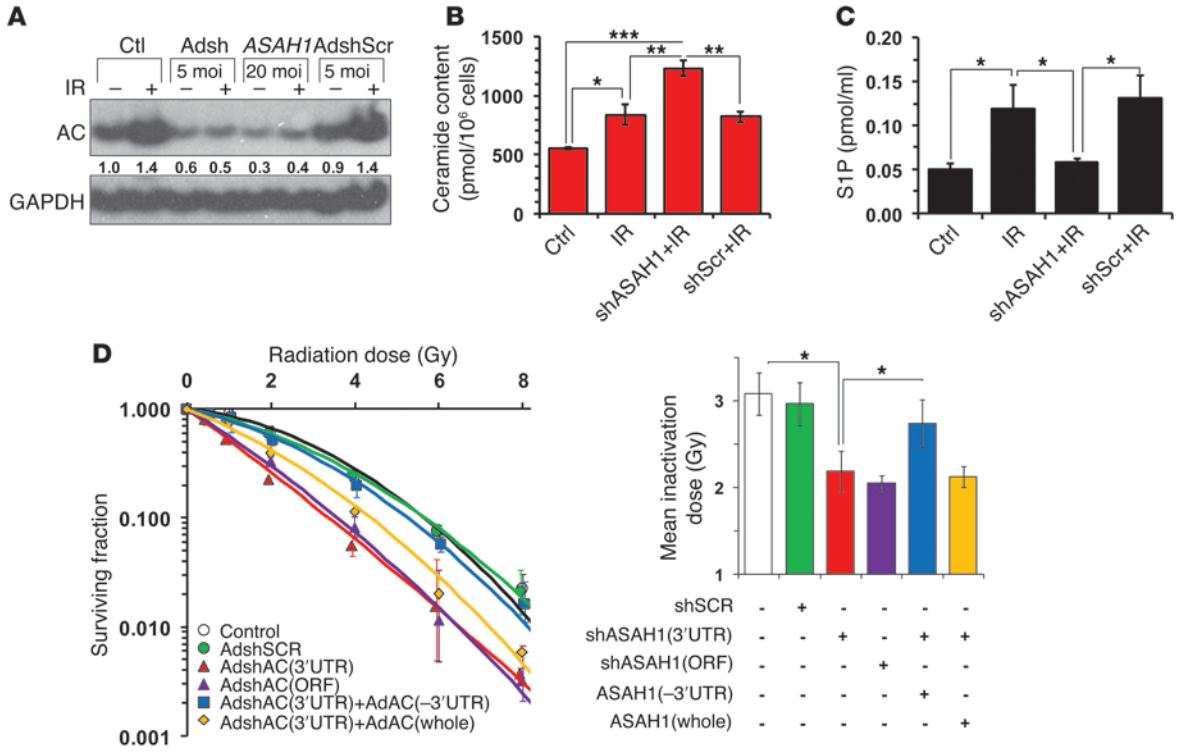

Figure 7

Targeting *ASAH1* increases PCa cell susceptibility to IR. (**A**) Protein expression in PPC-1 cells pretreated with Adsh*ASAH1* or AdshSCR vectors and γ irradiated (5 Gy, 48 hours). Mean densitometry of normalized AC expression is shown. (**B**) Sphingolipid content of Ad-transduced cells and (**C**) cell culture supernatants was analyzed by LC/MS 24 hours after IR (5 Gy). (**D**) Clonogenic survival of PPC-1 cell lines pretreated with Adsh*ASAH1* (AdshAC; targeting either *ASAH1* 3′UTR or ORF) or AdshSCR and γ irradiated between 0.5 and 8.0 Gy. Phenotypic rescue of radiosensitization was attempted with cotransduction with *ASAH1* overexpression vectors (AdAC; whole or 3′UTR deleted; see Methods). Results are shown as geometric mean ± SEM (left panels) and fitted to the linear-quadratic model to quantify mean inactivation dose (right panel). $^*P < 0.05$, $^{**}P < 0.01$, $^{***}P < 0.001$.

AC up to 8 weeks after the cessation of radiotherapy — 80%, 89%, and 64% respectively — while only 22% of PPC-1–TAM67 subclones overexpressed AC (Figure 6, C and D). Interestingly, the levels of AC expression in IR-surviving PPC-1 subclones, quantified by densitometry and normalized to GAPDH, correlated inversely with intracellular ceramide levels (Figure 6E) and correlated positively with radiation resistance (Figure 6F) and cell proliferation rate (Figure 6G). These results pointed to a significant role for AC in the phenotype of aggressive cancer cells that survive radiation therapy and repopulate the tumor.

We then formed the hypothesis that human prostate tissues of patients who have undergone and failed definitive radiation therapy may demonstrate higher levels of AC expression. Indeed, when examining the AC protein expression of archival prostate tissues from patients who suffered biochemical failure ($n = 8$), we found a significantly higher level of AC expression than in therapy-naive adenocarcinoma ($n = 30$; $P = 0.006$), prostatic intraepithelial neoplasia (PIN; $n = 26$; $P < 0.001$), or benign prostate tissues ($n = 27$; $P < 0.001$; Figure 6, H–L).These analyses also included 3 pairs of patient-matched PCa tissues before radiation therapy (Figure 6K) and after diagnosis of failure (Figure 6L), which demonstrated increased AC expression (Figure 6H). Taken together, these data not only confirm AC overexpression in frank prostatic adenocarcinoma, as observed previously by immunoblot (60) and RT-PCR (61), but also suggest that further enhancement of expression in response to therapy proffers a selective advantage to PCa cells under irradiative stress. Therefore, it was of keen interest to determine whether AC is a tractable target for combination therapy to improve PCa treatment with IR.

RNAi or lysosomotropic small molecule inhibition of AC sensitizes PCa cells to γ irradiation in vitro and in vivo. To test the hypothesis that AC ablation improves IR response in PCa cells, we transduced PPC-1 cells with adenoviral *ASAH1* shRNA targeting the 3′ UTR (Adsh$ASAH1_{3'UTR}$-GFP, 5 MOI) prior to γ irradiation. IR-induced AC upregulation was abrogated in cells transduced with Adsh$ASAH1_{3'UTR}$-GFP but not scrambled-sequence vector control (AdshSCR-GFP; Figure 7A). sh*ASAH1* expression resulted in enhanced accumulation of IR-induced ceramide (Figure 7B) and diminished S1P concentration in the cell culture supernatant (Figure 7C). Moreover, sh*ASAH1* transduction into PPC-1, 22Rv1, DU 145, and LNCaP cell lines significantly enhanced susceptibility in each case to IR-mediated clonogenic cell death (Figure 7D and Supplemental Figure 9). These results recapitulate our previous observations using transient transfection of siRNA against *ASAH1* to sensitize PCa cells to IR (49). Moreover, we transduced another shRNA construct, targeted toward the *ASAH1* ORF, and found similarly effective radiosensitization (Figure 7D). Reversal of the radiosensitization phenotype, with transgenic expression of Adsh$ASAH1_{3'UTR}$-GFP, was attempted with transgenic expression of *ASAH1*,

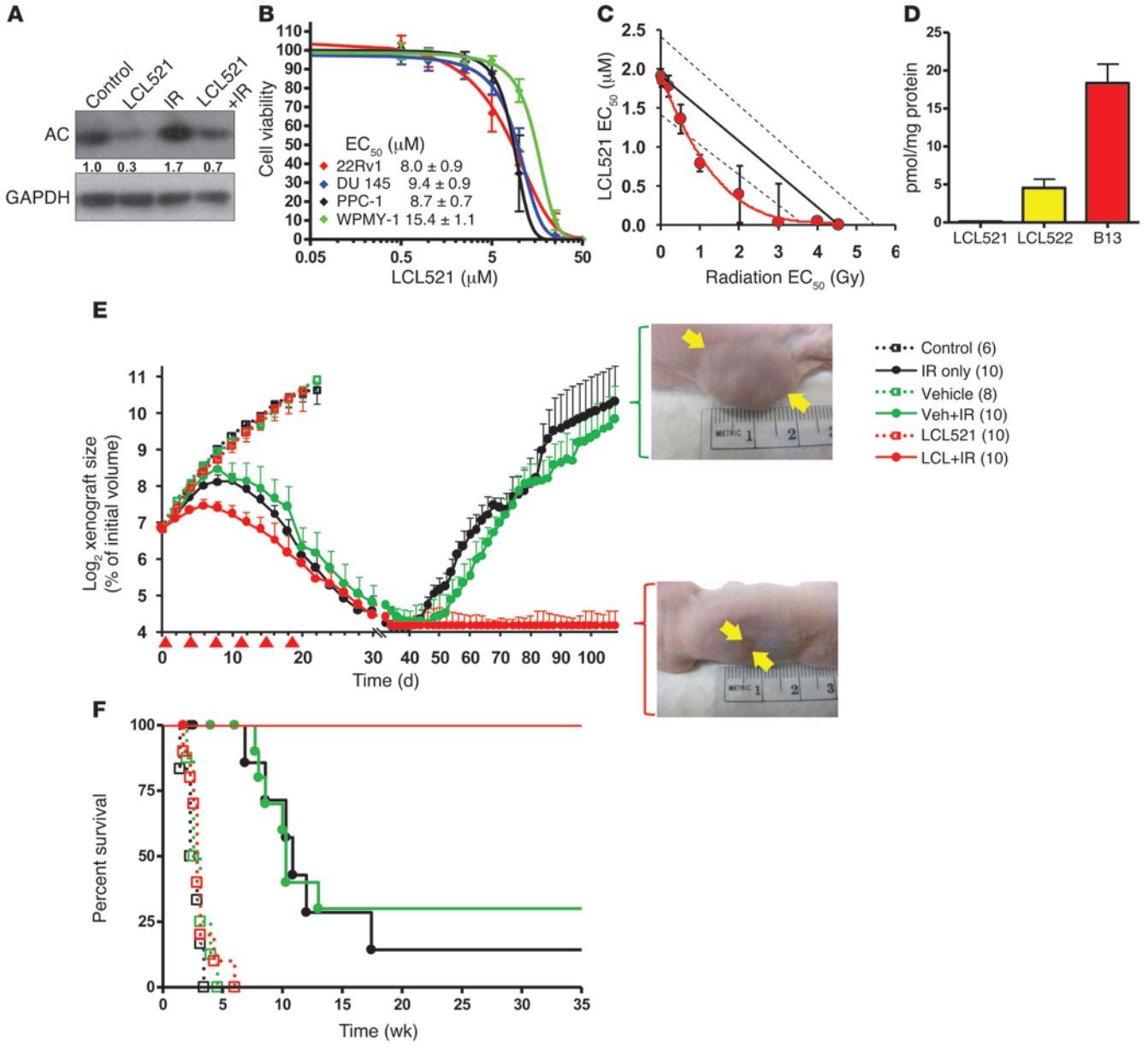

Figure 8

Radiosensitization of PCa IR via AC inhibition. (**A**) Protein expression in PPC-1 cells treated with AC small molecule inhibitor LCL521 (5 μM, 24 hours). Mean densitometry of normalized AC expression is shown. (**B**) 72-hour-dose responses of 22Rv1, DU 145, PPC-1, and WPMY-1 cell lines to LCL521 exposure. (**C**) Isobologram of LCL521 and IR combination therapy based on PPC-1 cell treatment for 8 days (single IR fraction at day 0; LCL521 treatment at days 0 and 4). Solid line represents theoretical line of additivity ± SD (dashed lines). (**D**) Ester bond hydrolysis of prodrug LCL521 into LCL522 and secondary ester bond hydrolysis into the active AC inhibitor, B13, in PPC-1 xenografts 6 hours after intraperitoneal administration (75 mg/kg). Subcutaneous PPC-1 xenografts grown on the flanks of athymic *nu/nu* mice were subjected to 6 × 5 Gy fractions of focal γ irradiation (red triangles) in combination with LCL521 (75 mg/kg, i.p. injection) or cremophor EL (vehicle control). (**E**) Xenograft volumes and (**F**) overall survival were monitored, and representative xenografts are depicted at day 108; *n* per group noted parenthetically.

with or without the 3′ UTR (Ad*ASAH1*$_{whole}$ and Ad*ASAH1*$_{-3'UTR}$, respectively; 10 MOI). Although Ad*ASAH1*$_{whole}$ expression did not reverse the sensitized phenotype, expression of the mutant Ad*ASAH1*$_{-3'UTR}$ restored the baseline response of PPC-1 cells to IR.

We demonstrated PCa cell sensitization to cytotoxic therapy and combination chemoradiation therapy via RNAi ablation of *ASAH1* in the context of paclitaxel (Taxol) administration as well. Measurement of ceramide species and sphingosine metabolites in PPC-1 cells exposed to paclitaxel (5 nM for 24 hours) demonstrated marked long-chain ceramide upregulation, without inducing significant changes of very-long-chain ceramide species, sphingosine, or S1P levels (Supplemental Figure 11A). These data suggested a sphingolipid profile shift toward a proapoptotic phenotype, as seen in Supplemental Figure 11D. Apoptosis induction by taxane therapy was abrogated by combination with IR exposure regardless of chemoradiation administration sequence (Sup-

plemental Figure 11C), indicating not only subadditive effect, but also possible antagonism between these anticancer modalities. However, pretreatment of cells with siRNA against *ASAH1* yielded increased PCa cell sensitivity to chemotherapy (Supplemental Figure 11, B and D). Moreover, the suppression of *ASAH1* expression produced optimal PCa cell sensitization to chemoradiation combination therapy (Supplemental Figure 11D).

Finally, small molecule inhibition of AC in vitro and in vivo was evaluated using a novel lysosomotropic prodrug inhibitor of AC, LCL521 (based on structural modification of the AC inhibitor B13; refs. 43, 62). LCL521 pretreatment of irradiated PPC-1 cells abrogated AC upregulation (Figure 8A). Singular treatment of prostate cell lines demonstrated susceptibility to LCL521 in the low micromolar range (Figure 8B), and combined modality treatment with γ irradiation demonstrated supra-additive PPC-1 cell killing in vitro (Figure 8C). Double-ester bond hydrolysis of the prodrug LCL521 into the active B13 was confirmed by LC/MS analyses of PPC-1–derived xenografts from *nu/nu* mice 6 hours after LCL521 treatment (intraperitoneal injection at 75 mg/kg; Figure 8D). Athymic *nu/nu* mice bearing subcutaneous PPC-1 cell xenografts (123 ± 4 mm^3) were given intraperitoneal LCL521 (75 mg/kg), or cremophor EL vehicle control, prior to charged particle irradiation under a schedule of fractionated irradiation (6×5 Gy; Figure 8E). Although LCL521 monotherapy produced no therapeutic benefit at this dose, marked response to the combination of LCL521 and IR was realized, compared with cremophor-infused (vehicle control) or untreated subjects. As shown in Figure 5, the cumulative dose of 30-Gy IR was insufficient to prevent xenograft relapse/regrowth. However, complete response was observed with IR in combination with LCL521 (Figure 8, E and F). Taken together, these results demonstrate that AC is a clinically relevant and druggable target for enhanced radiotherapeutic control of PCa.

Discussion

This study demonstrates that AC upregulation is a conserved response to radiation therapy across multiple tumor types and AC inhibition can directly improve the clinical response to radiotherapy in vitro and in vivo. IR exposure induced AC upregulation at the mRNA, protein, and enzyme activity level. Dependence of this process on ceramide expression was confirmed by exogenously or endogenously manipulating ceramide levels as well as suppression of IR-stimulated ceramide biogenesis. This observation led to our hypothesis that a critical threshold of intracellular ceramide exists beyond which a mechanism of AC gene transactivation is evoked in order to temper ceramide-mediated cell death. A transcription factor activity array and subsequent RNAi validation revealed that the c-Jun/AP-1 transcription factor significantly induces upregulation of AC following IR through de novo ceramide generation. In our hands, 90 percent of surviving clonal cell populations after 80-Gy IR overexpressed AC, and the level of AC expression correlated positively with proliferation and subsequent radiation insensitivity. Human prostate tissues, in addition to exhibiting AC upregulation in the tumor compared with benign tissues or PIN lesions, had significantly higher levels of AC following radiation therapy failure. In murine xenograft models, interference of AC gene transcription by the TAM67 dominant-negative mutant of c-Jun, RNAi against the AC gene, or lysosomotropic small molecule inhibition of the AC enzyme improved the therapeutic response to IR. Importantly, experiments with combination IR and LCL521 therapy provided a durable cure following completion of therapy. Finally, we demonstrated by in vitro clonogenic studies that rescue of AC overexpression in cells with endogenous AC suppression restored radioresistance and relapse following IR therapy proving the importance of this enzyme in the resistance pathway.

Curiously, the AC upregulation induced by radiation exposure in numerous adenocarcinoma and squamous cell carcinoma cell lines was not recapitulated in 3 noncancer prostate cell lines we evaluated: primary prostate epithelium (PrEC), immortalized prostate epithelium (PWR-1E), and immortalized prostate stroma cells (WPMY-1) (as seen in Supplemental Figure 8). Profiling the ceramide species of irradiated (5 Gy) and mock-irradiated cells revealed differences in total ceramide expression and relative species levels between the noncancer and cancer cell lines. These results suggest associations between a 2-fold increase of the overall intracellular ceramide burden, and/or specifically among the C_{16}-ceramide species, and AC induction. Investigations to distinguish differences in sphingolipid profile expression between "normal" versus malignant cells at baseline or in vitro growth conditions have identified higher levels of ceramide expression in cancer tissues and cells as well as species-specific variations (63, 64). At the level of enzymatic function, elucidating the control of sphingolipids upon chemotherapeutic or radiotherapeutic challenge may yield novel differences between cell types (65–70). This offers the tantalizing possibility that a distinct difference in sphingolipid regulation at clinically relevant IR dosage presents targets for therapeutic enhancement. Work in this laboratory is currently invested in identifying the underpinnings of such differential responses.

The mechanisms and pathways of irradiation-induced cell death in PCa cells are critical avenues of investigation. Canonical pathways of cell death would include the well-characterized pathway of de novo ceramide accumulation subsequent to irradiation supported by the findings of the Kolesnick group and others (23, 38, 51, 71, 72). The Kolesnick group characterized this de novo ceramide generation pathway in HeLa cells as dependent on CerS5/6 activation (70). Initial observations indicating that similar ceramide generation pathways were functioning in the PCa cells included the delayed and sustained onset of ceramide accumulation consistent with de novo ceramide synthesis rather than induction of ceramide accumulation through the action of sphingomyelinase. Ceramide accumulation was positively correlated with radiation dose and sensitivity to radiation, as evaluated by clonogenic assay. Furthermore, inhibition of both ceramide synthases with FB1 (51, 72) and the de novo pathway with myriocin (52) prevented IR-induced AC upregulation, ceramide generation, and IR-induced caspase activity, whereas inhibition of acid sphingomyelinase had no effect. Thus, we appear to be observing the diminution of proapoptotic ceramide signaling by ceramide-mediated induction of AC, an enzyme with demonstrated oncogenic activity in PCa (42), which in turn directly catabolizes ceramide itself.

We sought to further characterize the pathways of cell death in response to irradiation in PCa cells. Radiation treatment of cells induces marked G_2/M arrest, with increased apoptotic cells in a dose- and time-dependent manner, as determined by annexin V staining. Caspase-3 activity was increased following irradiation, with activity augmented by siRNA inhibition of AC. Apoptotic cell death mediated by de novo ceramide accumulation critically functions in mediating cell death following irradiation. Inhibition of necrotic cell death did not rescue IR-induced cell death in PPC-1 cells, suggesting that necrosis, unlike apoptosis, does not appear to be the major cell death pathway in this setting. Although we

identified the cell death pathway following IR through de novo ceramide generation and apoptosis augmented by the inhibition of AC, we have not yet ruled out a contribution of mitotic catastrophe mediated by factors such as caspase-2. This mechanism of IR-induced cell damage/death is of great interest to us, as ceramide may be of importance to this process (73).

Although the onset of ceramide accumulation would predict a favorable outcome to therapy, due to ceramide's roles in apoptosis and growth arrest, we also observed substantial increases in the ceramide catabolite sphingosine and its anabolite S1P. As free sphingosine is mainly produced by deacylation of ceramide, this observation was highly suggestive of increased flux through 1 or more of the 5 human ceramidases. Interestingly, we found that AC was increased specifically, with no significant alteration in activity or mRNA expression of neutral or alkaline ceramidases. This may be due, in part, to the increase of C_{16}-ceramide — a preferred substrate of AC (44) — relative to other species under conditions radiation exposure or exogenous ceramide treatment. We might also posit that the wave of autophagic activity engendered by a dose of IR that is not immediately lethal accounts for a conserved induction of lysosomal components (74, 75), of which AC is a significant member. How this process may be connected to IR-stimulated c-Jun/AP-1 activity (76, 77) remains underappreciated (78) and an important matter for investigation. In addition, no significant change of sphingosine kinase activity in irradiated PPC-1/PC-3 cells (49, 79) coincides with IR-induced AC, which led to our hypothesis that AC represents a rate-limiting step for IR-induced ceramide catabolism.

Ceramide is a pleiotropic signaling lipid and IR induces myriad alterations to cellular signaling (as reviewed in ref. 80). Mechanistically, we were interested to find that inhibition of ceramide generation following IR by pretreatment with FB1 or myriocin prevented not only ceramide accumulation, but also upregulation of AC transcription and protein expression. This observation lead to the hypothesis that ceramide generation induces AC upregulation as a feedback mechanism to dampen the apoptotic ceramide signal. Moreover, the rapid catabolism of stress-induced ceramide into mitogenic/oncogenic S1P counteracts apoptosis signaling propagated by ceramide accumulation (17). Intriguingly, we observed that nonmalignant prostate epithelial and stromal cell lines do not upregulate AC with IR exposure, which may reveal a survival mechanism that contributes to evasion of apoptosis in malignant cells, as opposed to the orderly apoptotic program maintained by normal cells.

A role for ceramide in regulating gene expression has long been appreciated (81–87). In order to seek out the transcriptional mechanism for IR-induced AC upregulation, we identified transcription factor alterations that were common to ceramide treatment and IR individually. Both ceramide and IR activated AP-1, and siRNA knockdown of the various Jun/Fos components indicated c-Jun involvement in these processes. c-Fos involvement was implicated as well, although results were shy of significance and, therefore, equivocal. Interestingly, JUNB binding was confirmed at the ASAH1 promoter as well, although the level of interaction between this protein and the promoter was unaffected by IR or C_6-ceramide induction. Also of note was the failure of myriocin to inhibit c-Jun or c-Fos binding stimulated by C_6-ceramide. These observations may result from the bypass of de novo ceramide generation achieved with the exogenous administration of a ceramide source, which may feed the recycling pathway of ceramide biosynthesis, mediated by FB1-sensitive ceramide synthases (88).

The c-Jun proto-oncogene has long been appreciated for mediating cellular transformation, growth, and angiogenesis (89–95) and may have more labile activity in malignant cells (96). The Kester group demonstrated that AP-1 transactivates neutral ceramidase in human coronary artery smooth muscle cells with stimulation by fetal bovine serum (97). Here, through a combination of luciferase reporter truncations/mutations and ChIP–RT-PCR, we deduced the node of c-Jun/AP-1 interaction with the *ASAH1* promoter to the –475/–468–bp site. It was suggested that AP-1 control of neutral ceramidase transcription is tightly regulated by predicted overlapping binding of NF-Y or interaction with proximate *cis*-binding factors, considerations that may direct context-dependent transcription of either neutral or AC under disparate stimuli. Investigation of other transcription factors regulating AC expression, such as CREB (54) and KLF6 (98), via RNAi studies have not yet revealed involvement of those particular factors in IR-induced AC upregulation (data not shown). However, it should be noted that in silico detection by TFBind of CREB, Stat-1, and Elk-1 consensus binding sequences on the same promoter region as AP-1 may suggest competition for or interaction of binding on the AC gene promoter under various conditions of stimulation.

Approximately 50% of patients with cancer undergo radiation therapy (99, 100), typically administered in fractionated doses up to 2 Gy every weekday for 7 to 8 weeks in order to avoid toxicity to adjacent structures (101). However, experimental models of fractionated radiation to clinically achievable doses remain underreported. In the present study, we attempted to mimic clinical irradiation of cancer cells, irradiating PCa cells in vitro at 2-Gy doses for 40 times for the cumulative IR dose of 80 Gy. In our analysis of the surviving clones, we were surprised to find that fractionated irradiation did not completely ablate the reproductive capacity of cancer cells, and, interestingly, 90% of these IR subclones continued to overexpress AC. Although neither the average radiation resistance nor proliferation rate of these IR subclones was as robust as therapy-naive cells, their levels of AC expression showed remarkable correlation with these parameters, harkening to the eventual biochemical failure and relapse of a proportion of radiotherapy patients. As seen in our animal studies using PPC-1 xenografts bearing a doxycycline-inducible AC expression cassette, irradiated mice with forced AC overexpression demonstrated a poorer response to IR compared with mice without AC induction. The irradiated mice overexpressing AC also exhibited earlier relapse compared with IR-treated mice with no AC induction, suggesting a significant contribution to therapy resistance. Taken together, these results demonstrate that AC supports a radioresistance phenotype and inform the hypothesis that enhanced AC expression would be found in prostate tumors that fail definitive courses of radiation therapy.

This was confirmed by evaluation of human prostate tissues by immunohistochemistry. These data suggest that AC is upregulated following IR and support the notion that AC may contribute to resistance and relapse. Retrospective analysis of tissues from difficult to obtain relapsed malignancies showed that radiotherapy patient samples have elevated AC expression. These data provide an indication that our in vitro interrogation of PCa cell responses to IR revealed valid findings. Future studies could use quantification of AC protein in human plasma, urine, or expressed prostatic secretions, which are amenable to high-throughput platforms and allow noninvasive evaluation of tumor response to IR and potential for relapse. This is an attrac-

tive approach to studying AC in cancer cells, as their enhanced autophagy and secretory activity enriches the extracellular concentration of lysosomal contents (102–104) and because AC can be detected and isolated from human urine (105).

Clinically achievable radiation doses are limited by systemic and local toxicity to adjacent structures. Thus, adjuvant therapy that selectively sensitizes tumors to IR might enable lower doses with lower adverse events. The efficacy of IR on xenografts with tightly controlled AC expression supports the notion of inhibiting AC as a strategy for improved cancer therapy. Indeed, our experiments indicate that targeting AC upregulation by interfering with c-Jun activation and by small molecule inhibition augments the efficacy of IR without an increase in total dose of radiation (Figures 4 and 5). Moreover, inhibition of AC with the novel lysosomotropic prodrug AC inhibitor, LCL521, prevented relapse (resumption of tumor growth after apparent eradication) in the mice (n = 10), whereas approximately 70% of mice receiving only IR experienced relapse. This situation recapitulates relapse after definitive radiation therapy in human patients with locally advanced disease, 50% of who ultimately experience recurrence of disease. These promising in vivo studies suggest that AC may be an ideal clinical target in the setting of solid tumor irradiation.

An important concern with radiosensitizing agents is the potential for sensitization of normal tissue or augmentation of systemic toxicity, effectively defeating the purpose of adjuvant therapy. Our studies indicate no increased toxicity in mice receiving IR plus LCL521 in comparison with that in the group receiving only LCL521. Although no benefit was observed for LCL521 as a single agent against tumor growth at the dose administrated, synergistic cell killing in combination with IR characterizes LCL521 as an efficacious radiosensitizer. Using our rationally designed AC inhibitors, a previous study demonstrated that susceptibility to AC inhibition corresponds to the level of basal AC expression in treated cells (106). This suggests that AC inhibition can produce greater therapeutic benefit in treated tumors, due to specific AC induction via focal IR delivery. Additional evaluation of radiosensitization of nontargeted tissue is necessary as we move forward with evaluation of this therapeutic modality; however, the specificity and lack of apparent unintended sensitization is encouraging. Additionally, while LCL521 is at this point highly experimental and its clinical feasibility is not well known (but currently under evaluation), our study clearly outlines a role for AC inhibition in radiosensitization of prostate tumors.

In summary, our data strongly support AC as a major factor in the development of radiation resistance in PCa therapy. Multiple methods clearly demonstrate that interference of AC induction and activity sensitizes cancer cells to IR in vitro and in vivo. Upregulation of AC in radiotherapy-relapsed human tumors confirms the described phenomenon and justifies further study into the feasibility and efficacy of targeting AC in patients receiving IR for PCa. Therefore, AC inhibition presents a rational approach for improving radiotherapy in the preclinical environment with the potential for advancement into patients.

Methods

Cell culture and reagents. The human prostate cell lines PPC-1 (gift of Yi Lu, University of Tennessee, Knoxville, Tennessee, USA), DU 145 (ATCC), PC-3 (ATCC), and CWR22Rv1 (ATCC) were maintained in RPMI 1640 media supplemented with 10% bovine growth serum and incubated in 5% CO_2 at 37°C. The LNCaP progression series of cell lines was a gift from Leland W.K. Chung (Cedars-Sinai Medical Center, Los Angeles, California, USA) and was cultured according to published methods (107, 108). Cell lines were validated in by STR profiling using the PowerPlex1.2 marker set. Enumeration of cells in any experiment was performed using a Scepter automated cell counter (Millipore), followed by confirmation of viability through Trypan blue exclusion. FB1 (Enzo Life Sciences no. BML-SL220) was dissolved in double-distilled H_2O to a concentration of 25 mM. Myriocin (Enzo Life Sciences no. BML-SL226) was dissolved in DMSO (to 10 mM). The MUSC Lipidomics Synthetic Core Facility provided C_6-ceramide, which was dissolved in DMSO (to 25 mM), and LCL521, which was dissolved in ethanol (to 50 mM). Solvent/vehicle administrations to cell cultures were conduct at dilutions of 1:1,000 or higher. Additional information is provided in the Supplemental Methods. Primer and RNAi nucleotide sequences are listed in Supplemental Tables 1 and 2.

In vitro cell culture irradiation. Cell cultures were irradiated in a ^{137}Cs γ-irradiator (J.L. Shepherd & Associates) at an average dose rate of 2.15 Gy per minute based on decay, as previously described (49). Dosimetry using radiochromic (self-developing) film was performed regularly to verify accuracy of delivery.

Small animal experiments. Athymic *nu/nu Mus musculus* (NCI Frederick) between 7 and 12 weeks of age were inoculated subcutaneously with 5×10^6 cells in a 1:1 RPMI 1640/Matrigel HC admixture (0.08 ml per injection). Animals were enrolled into studies upon establishment of flank xenografts >100 mm^3. Doxycycline administration consisted of feeding animals 250 mg/l doxycycline in 2% sucrose water, which was refreshed every 2 days. Combined modality therapy with LCL521 administration constituted intraperitoneal delivery of drug dissolved in 1:2 cremophor EL/saline solution to a dose of 75 mg/kg per animal. Two to four hours after injection, animals were subjected to sham or focal charged-particle irradiation delivered with a 9-MeV electron beam generated by a Varian 2100EX linear accelerator with dosing prescribed to a depth of 1 cm. Mice were anesthetized and positioned in individual slots of a custom-designed scaffold. A 5-mm-thick custom lead shield was used to protect the normal tissue of the mice. Circular windows of either 1.25-cm or 1.75-cm diameters drilled into the lead shield exposed 1.0-cm or 1.5-cm diameter tumors, respectively. The mice were placed 100 cm from the radiation source, and a 1.0-cm tissue-equivalent bolus (Superflab) was placed on top of the tumors to provide sufficient dose build up. Dosimetry was verified using radiochromic (self-developing) film prior to irradiation. Tumor volumes were measured every 48 hours with digital calipers (Fisher) and recorded as volume (mm^3) = [4π/3] × length × width × depth. Animal weight was monitored, and tumor xenografts growing larger than 2,000 mm^3 or developing ulcers were considered as having reached the end point; all other events removing animals from the studies were considered censored events.

Sphingolipid analysis. Ceramides species, sphingosine, and S1P from cell pellets, culture supernatants, and xenograft homogenates were collected and analyzed with LC-MS/MS by the Lipidomics Shared Resource, MUSC, as previously described (49). Synthesis of the AC inhibitors, LCL521, LCL522, and B13, was conducted in the Lipidomics Shared Resource.

Adenoviral vectors. Adenoviral vectors expressing CMV-driven CerS6 were designed by Christina Voelkl-Johnson and Tejas Tirodkar and were manufactured by Vector Biolabs. They also provided anti-CerS6 antibody (Abnova). CMV-driven Ad*ASAH1*$_{whole}$-GFP and Ad*ASAH1*-$_{3'UTR}$-GFP and U6-driven Adsh*ASAH1*$_{3'UTR}$-GFP and Adsh*ASAH1*$_{ORF}$-GFP were developed by Open Biosystems and Vector Biolabs. CMV-driven Ad-GFP (no. 1060) and U6-driven Ad-shScr-GFP (no. 1122) control adenoviral vectors were obtained from Vector Biolabs.

Enzyme activity assays. Assays for ceramidase activities were performed as previously described (109, 110).

Western blot. Immunoblot analyses of cell lysates were performed as previously described (49) using antibodies to detect AC (BD Transduction no. 612302), CerS6 (gift of C. Voelkl-Johnson), β-actin (Sigma-Aldrich no. A5441), and GAPDH (Santa Cruz Biotechnology, no. sc-32233).

Transcription factor activity assay. Protein-DNA complexes were isolated using a Nuclear Extraction Kit (Affymetrix no. AY2002) and evaluated by the Protein/DNA Array I according to manufacturer's instructions (Affymetrix no. MA1210). Protein-bound DNA probes are hybridized to the array and assessed by chemiluminescence. Signal intensity data are quantified by densitometry using Quantity One software (Bio-Rad).

Reporter gene construction. We cloned 1.5 kb of the human *ASAH1* promoter (NCBI accession AF220172) using the following primers: forward 5′-GATCCTCGAGCTCCACTGCATTTGTCAC-3′, reverse 5′-GATCTGATCAATCGCTCTAGCAGCCAAC-3′. The amplified product was ligated into the *XhoI* (5′) and *BamHI* (3′) cloning site of the pLVX-Luc vector (Clontech no. 632162) occupied by the P_{Tight} promoter. Stable expression of the reporter construct, p*ASAH1*-Luc, or the control pLVX-Luc vector was established by culturing transfectants under puromycin selection conditions per manufacturer's instructions. Firefly luciferase activity was measured with the Bright-Flo Luciferase assay kit (Promega) in 96-well microtiter plates using 10^4 cells per well. Luminosity was measured by a FLUOstar Optima plate reader (BMG), and data shown represent the integration of 10 minutes of luciferase readings during the plateau phase of luciferase activity.

Clonogenic survival assay. Clonogenic survival was assessed as previously described (49). Briefly, cells in each treatment group were plated in triplicate into 35-mm culture plates after IR. After 10 to 14 days of culture, cells were fixed in 3.7% formaldehyde and stained in 1.0% crystal violet and 0.5% acetic acid, whereupon colonies of ≥50 cells were enumerated. Data representing geometric mean ± SEM were fitted to the linear-quadratic model, and the mean inactivation dose was calculated according to Fertil et al. (111).

Immunohistochemistry. Paraffin-embedded formalin-fixed human prostate specimens were evaluated for AC protein expression as previously described (102). Briefly, anti-AC primary antibody (1:100; Santa Cruz Biotechnology, sc-100646) or IgG_3 control was diluted with DAKO antibody diluent, added to the slides, and incubated at 4°C overnight. A biotinylated link antibody along with a streptavidin biotin peroxidase kit (DakoLSABþ System-HRP) was then used along with a DAB chromogen and peroxide substrate to detect the bound antibody complexes. The slides were counterstained with hematoxylin and dehydrated through graded alcohols to xylene. A pathologist, blinded to tissue identity, scored 3 areas per tissue core and evaluated them using the following scale: 0, no staining of any cells; 1, faint staining; 2, moderate intensity staining; and 3–5, intense staining.

Statistics. Unless otherwise indicated, data represent mean ± SEM of 3 independent experiments (n = 3) and were tested for statistical significance by 1-way ANOVA and Tukey-Kramer post-hoc analysis, assuming $\alpha = 0.05$, with GraphPadInstat 3. Pairwise comparisons of only 2 data groups were subjected to nonparametric analysis of statistical significance (Mann-Whitney U test). For xenograft experiments, differences in average fold change between groups were evaluated on the log scale using 2 sample t tests, with a P value of less than 0.05 considered statistically significant.

Study approval. Archived, deidentified human tissues were obtained and evaluated under the auspices of Medical University of South Carolina Institutional Review Board protocols HR20613 and NHR397. Animal care, handling, and experiments were conducted under the auspices of Medical University of South Carolina Institutional Animal Care and Use Committee protocol AR1575.

Acknowledgments

This work was funded by NCI P01CA097132-07 (to J.S. Norris) and NCRR UL1 RR029882 (South Carolina Clinical and Translational Research Institute). Support to the Lipidomics Core Facility, Biorepository and Research Pathology Services, and Biostatistics and Clinical Trials Shared Resource was provided by NCI P30 CA138313 (Hollings Cancer Center). Animal projects were conducted in a facility constructed with support from NCRR C06 RR015455. For their technical assistance, the authors give thanks to Lori Turner, David Holman, Sherry Zhou, William Meacham, Marisa Meyers-Needham, Cynthia Schandl, Laura Colombo, Kiki Gibbs, Ken Vanek, and Liya Zhou. The authors are indebted to Christina Voelkel-Johnson and Tejas Tirodkar for the AdCerS6-GFP vector and anti-CerS6 antibody; Marion Sewer for pGL3-p*ASAH1*-Luc constructs; Michael Birrer for the pcDNA3-TAM67 construct; Jacek Bielawski for LC-MS/MS lipid analyses; Angen Liu for blinded immunohistochemistry scoring; and Yusuf Hannun, Dennis Watson, Keith Kirkwood, Besim Ogretmen, Elizabeth Garrett-Mayer, Xiaoyi Zhang, and Jennifer Wu for critical input.

Received for publication May 14, 2012, and accepted in revised form July 11, 2013.

Address correspondence to: James S. Norris, Department of Microbiology and Immunology, Medical University of South Carolina, 173 Ashley Avenue, Charleston, South Carolina 29425, USA. Phone: 843.792.7915; Fax: 843.792.4882; E-mail: norrisjs@musc.edu.

1. Nguyen PL, et al. Cost implications of the rapid adoption of newer technologies for treating prostate cancer. *J Clin Oncol*. 2011;29(12):1517–1524.
2. Sheets NC, et al. Intensity-modulated radiation therapy, proton therapy, or conformal radiation therapy and morbidity and disease control in localized prostate cancer. *JAMA*. 2012;307(15):1611–1620.
3. National Comprehensive Cancer Network. National Comprehensive Cancer Network Clinical Practice Guidelines in Oncology: Prostate Cancer, Version 1.2013. NCCN Web site. http://www.nccn.org/professionals/physician_gls/f_guidelines.asp#prostate. Accessed July 31, 2013.
4. Vora SA, et al. Outcome and toxicity for patients treated with intensity modulated radiation therapy for localized prostate cancer. *J Urol*. 2013;190(2):521–526.
5. Kupelian PA, Buchsbaum JC, Elshaikh MA, Reddy CA, Klein EA. Improvement in relapse-free survival throughout the PSA era in patients with localized prostate cancer treated with definitive radiotherapy: year of treatment an independent predictor of outcome. *Int J Radiat Oncol Biol Phys*. 2003;57(3):629–634.
6. Gutt R, Tonlaar N, Kunnavakkam R, Karrison T, Weichselbaum RR, Liauw SL. Statin use and risk of prostate cancer recurrence in men treated with radiation therapy. *J Clin Oncol*. 2010;28(16):2653–2659.
7. Alicikus ZA, et al. Ten-year outcomes of high-dose, intensity-modulated radiotherapy for localized prostate cancer. *Cancer*. 2011;117(7):1429–1437.
8. Spratt DE, Pei X, Yamada J, Kollmeier MA, Cox B, Zelefsky MJ. Long-term survival and toxicity in patients treated with high-dose intensity modulated radiation therapy for localized prostate cancer. *Int J Radiat Oncol Biol Phys*. 2013;85(3):686–692.
9. Kupelian PA, Willoughby TR, Reddy CA, Klein EA, Mahadevan A. Hypofractionated intensity-modulated radiotherapy (70 Gy at 2.5 Gy per fraction) for localized prostate cancer: Cleveland Clinic experience. *Int J Radiat Oncol Biol Phys*. 2007;68(5):1424–1430.
10. Bolla M, et al. Long-term results with immediate androgen suppression and external irradiation in patients with locally advanced prostate cancer (an EORTC study): a phase III randomised trial. *Lancet*. 2002;360(9327):103–106.
11. Kuban DA, et al. Long-term results of the M. D. Anderson randomized dose-escalation trial for prostate cancer. *Int J Radiat Oncol Biol Phys*. 2008;70(1):67–74.
12. Dearnaley DP, et al. Escalated-dose versus standard-dose conformal radiotherapy in prostate cancer: first results from the MRC RT01 randomised controlled trial. *Lancet Oncol*. 2007;8(6):475–487.
13. Zietman AL, et al. Comparison of conventional-dose vs high-dose conformal radiation therapy in clinically localized adenocarcinoma of the prostate. *JAMA*. 2005;294(10):1233–1239.
14. Chism DB, Horwitz EM, Hanlon AL, Pinover WH, Mitra RK, Hanks GE. Late morbidity profiles in prostate cancer patients treated to 79-84 Gy by a simple four-field coplanar beam arrangement. *Int J Radiat Oncol Biol Phys*. 2003;55(1):71–77.
15. Smit WG, Helle PA, van Putten WL, Wijnmaalen AJ, Seldenrath JJ, van der Werf-Messing BH. Late radiation damage in prostate cancer patients treated by high dose external radiotherapy in relation to rectal dose. *Int J Radiat Oncol Biol Phys*. 1990;18(1):23–29.
16. Lawton CA, et al. Long-term treatment sequelae following external beam irradiation for adenocarcinoma of the prostate: analysis of RTOG studies 7506 and 7706. *Int J Radiat Oncol Biol Phys*. 1991;21(4):935–939.
17. Cuvillier O, et al. Suppression of ceramide-mediated programmed cell death by sphingosine-1-

phosphate. *Nature*. 1996;381(6585):800–803.
18. Ogretmen B, Hannun YA. Biologically active sphingolipids in cancer pathogenesis and treatment. *Nat Rev Cancer*. 2004;4(8):604–616.
19. Hannun YA, Obeid LM. Principles of bioactive lipid signalling: lessons from sphingolipids. *Nat Rev Mol Cell Biol*. 2008;9(2):139–150.
20. Morad SA, Cabot MC. Ceramide-orchestrated signalling in cancer cells. *Nat Rev Cancer*. 2013; 13(1):51–65.
21. Adan-Gokbulut A, Kartal-Yandim M, Iskender G, Baran Y. Novel agents targeting bioactive sphingolipids for the treatment of cancer. *Curr Med Chem*. 2013;20(1):108–122.
22. Beckham TH, Cheng JC, Marrison ST, Norris JS, Liu X. Interdiction of sphingolipid metabolism to improve standard cancer therapies. *Adv Cancer Res*. 2013;117:1–36.
23. Vit JP, Rosselli F. Role of the ceramide-signaling pathways in ionizing radiation-induced apoptosis. *Oncogene*. 2003;22(54):8645–8652.
24. Kimura K, Markowski M, Edsall LC, Spiegel S, Gelmann EP. Role of ceramide in mediating apoptosis of irradiated LNCaP prostate cancer cells. *Cell Death Differ*. 2003;10(2):240–248.
25. Deng X, et al. Ceramide biogenesis is required for radiation-induced apoptosis in the germ line of C. elegans. *Science*. 2008;322(5898):110–115.
26. Hara S, et al. p53-Independent ceramide formation in human glioma cells during [gamma]-radiation-induced apoptosis. *Cell Death Differ*. 2004; 11(8):853–861.
27. Haimovitz-Friedman A, et al. Ionizing radiation acts on cellular membranes to generate ceramide and initiate apoptosis. *J Exp Med*. 1994;180(2):525–535.
28. Verheij M, et al. Requirement for ceramide-initiated SAPK/JNK signalling in stress-induced apoptosis. *Nature*. 1996;380(6569):75–79.
29. Chmura SJ, Nodzenski E, Beckett MA, Kufe DW, Quintans J, Weichselbaum RR. Loss of ceramide production confers resistance to radiation-induced apoptosis. *Cancer Res*. 1997;57(7):1270–1275.
30. Chmura SJ, et al. Down-regulation of ceramide production abrogates ionizing radiation-induced cytochrome c release and apoptosis. *Mol Pharmacol*. 2000;57(4):792–796.
31. Santana P, et al. Acid sphingomyelinase-deficient human lymphoblasts and mice are defective in radiation-induced apoptosis. *Cell*. 1996;86(2):189–199.
32. Bruno AP, et al. Lack of ceramide generation in TF-1 human myeloid leukemic cells resistant to ionizing radiation. *Cell Death Differ*. 1998;5(2):172–182.
33. Bonnaud S, et al. Sphingosine-1-phosphate activates the AKT pathway to protect small intestines from radiation-induced endothelial apoptosis. *Cancer Res*. 2010;70(23):9905–9915.
34. Otala M, et al. Protection from radiation-induced male germ cell loss by sphingosine-1-phosphate. *Biol Reprod*. 2004;70(3):759–767.
35. Morita Y, et al. Oocyte apoptosis is suppressed by disruption of the acid sphingomyelinase gene or by sphingosine-1-phosphate therapy. *Nat Med*. 2000;6(10):1109–1114.
36. Samsel L, et al. The ceramide analog, B13, induces apoptosis in prostate cancer cell lines and inhibits tumor growth in prostate cancer xenografts. *Prostate*. 2004;58(4):382–393.
37. Alphonse G, Bionda C, Aloy MT, Ardail D, Rousson R, Rodriguez-Lafrasse C. Overcoming resistance to gamma-rays in squamous carcinoma cells by polydrug elevation of ceramide levels. *Oncogene*. 2004; 23(15):2703–2715.
38. Kolesnick R, Fuks Z. Radiation and ceramide-induced apoptosis. *Oncogene*. 2003;22(37):5897–5906.
39. McDermott U, Downing JR, Stratton MR. Genomics and the continuum of cancer care. *N Engl J Med*. 2011;364(4):340–350.
40. Elojeimy S, et al. Role of acid ceramidase in resistance to FasL: therapeutic approaches based on acid ceramidase inhibitors and FasL gene therapy. *Mol Ther*. 2007;15(7):1259–1263.
41. Gouaze-Andersson V, et al. Inhibition of acid ceramidase by a 2-substituted aminoethanol amide synergistically sensitizes prostate cancer cells to N-(4-hydroxyphenyl) retinamide. *Prostate*. 2011;71(10):1064–1073.
42. Saad AF, et al. The functional effects of acid ceramidase overexpression in prostate cancer progression and resistance to chemotherapy. *Cancer Biol Ther*. 2007;6(9):1455–1460.
43. Szulc ZM, et al. Novel analogs of d-e-MAPP and B13. Part 1: Synthesis and evaluation as potential anticancer agents. *Bioorg Med Chem*. 2008; 16(2):1015–1031.
44. Bielawska A, et al. Novel analogs of d-e-MAPP and B13. Part 2: Signature effects on bioactive sphingolipids. *Bioorg Med Chem*. 2008;16(2):1032–1045.
45. Liu X, et al. Modulation of ceramide metabolism enhances viral protein apoptin's cytotoxicity in prostate cancer. *Mol Ther*. 2006;14(5):637–646.
46. Eto M, Bennouna J, Hunter OC, Lotze MT, Amoscato AA. Importance of C16 ceramide accumulation during apoptosis in prostate cancer cells. *Int J Urol*. 2006;13(2):148–156.
47. Noda S, et al. Role of ceramide during cisplatin-induced apoptosis in C6 glioma cells. *J Neurooncol*. 2001;52(1):11–21.
48. Hara S, et al. Ceramide triggers caspase activation during gamma-radiation-induced apoptosis of human glioma cells lacking functional p53. *Oncol Rep*. 2004;12(1):119–123.
49. Mahdy AE, et al. Acid ceramidase upregulation in prostate cancer cells confers resistance to radiation: AC inhibition, a potential radiosensitizer. *Mol Ther*. 2009;17(3):430–438.
50. Thomas RL, Matsko CM, Lotze MT, Amoscato AA. Mass spectrometric identification of increased C16 ceramide levels during apoptosis. *J Biol Chem*. 1999;274(43):30580–30588.
51. Wang E, Norred WP, Bacon CW, Riley RT, Merrill AH. Inhibition of sphingolipid biosynthesis by fumonisins. Implications for diseases associated with Fusarium moniliforme. *J Biol Chem*. 1991; 266(22):14486–14490.
52. Horvath A, Sutterlin C, Manning-Krieg U, Movva NR, Riezman H. Ceramide synthesis enhances transport of GPI-anchored proteins to the Golgi apparatus in yeast. *EMBO J*. 1994;13(16):3687–3695.
53. Hurwitz R, Ferlinz K, Sandhoff K. The tricyclic antidepressant desipramine causes proteolytic degradation of lysosomal sphingomyelinase in human fibroblasts. *Biol Chem Hoppe Seyler*. 1994; 375(7):447–450.
54. Lucki N, Sewer MB. The cAMP responsive element binding protein (CREB) regulates the expression of acid ceramidase (ASAH1) in H295R human adrenocortical cells. *Biochim Biophys Acta*. 2009; 1791(8):706–713.
55. Lucki NC, Bandyopadhyay S, Wang E, Merrill AH, Sewer MB. Acid ceramidase (ASAH1) is a global regulator of steroidogenic capacity and adrenocortical gene expression. *Mol Endocrinol*. 2012; 26(2):228–243.
56. Brown PH, Alani R, Preis LH, Szabo E, Birrer MJ. Suppression of oncogene-induced transformation by a deletion mutant of c-jun. *Oncogene*. 1993; 8(4):877–886.
57. Domann FE, Levy JP, Birrer MJ, Bowden GT. Stable expression of a c-JUN deletion mutant in two malignant mouse epidermal cell lines blocks tumor formation in nude mice. *Cell Growth Differ*. 1994; 5(1):9–16.
58. Dong Z, et al. A dominant negative mutant of jun blocking 12-O-tetradecanoylphorbol-13-acetate-induced invasion in mouse keratinocytes. *Mol Carcinog*. 1997;19(3):204–212.
59. Bedia C, Casas J, Andrieu-Abadie N, Fabrias G, Levade T. Acid ceramidase expression modulates the sensitivity of A375 melanoma cells to dacarbazine. *J Biol Chem*. 2011;286(32):28200–28209.
60. Norris JS, et al. Combined therapeutic use of AdGFPFasL and small molecule inhibitors of ceramide metabolism in prostate and head and neck cancers: a status report. *Cancer Gene Ther*. 2006; 13(12):1045–1051.
61. Seelan RS, Qian C, Yokomizo A, Bostwick DG, Smith DI, Liu W. Human acid ceramidase is overexpressed but not mutated in prostate cancer. *Genes Chromosomes Cancer*. 2000;29(2):137–146.
62. Selzner M, et al. Induction of apoptotic cell death and prevention of tumor growth by ceramide analogues in metastatic human colon cancer. *Cancer Res*. 2001;61(3):1233–1240.
63. Saddoughi SA, et al. Results of a phase II trial of gemcitabine plus doxorubicin in patients with recurrent head and neck cancers: serum C(1)(8)-ceramide as a novel biomarker for monitoring response. *Clin Cancer Res*. 2011;17(18):6097–6105.
64. Koybasi S, et al. Defects in cell growth regulation by C18:0-ceramide and longevity assurance gene 1 in human head and neck squamous cell carcinomas. *J Biol Chem*. 2004;279(43):44311–44319.
65. Siddique MM, et al. Ablation of dihydroceramide desaturase confers resistance to etoposide-induced apoptosis in vitro. *PLoS One*. 2012;7(9):e44042.
66. Liao WC, et al. Ataxia telangiectasia-mutated gene product inhibits DNA damage-induced apoptosis via ceramide synthase. *J Biol Chem*. 1999; 274(25):17908–17917.
67. Cheng Y, et al. Identification of aberrant forms of alkaline sphingomyelinase (NPP7) associated with human liver tumorigenesis. *Br J Cancer*. 2007; 97(10):1441–1448.
68. Brizuela L, Ader I, Mazerolles C, Bocquet M, Malavaud B, Cuvillier O. First evidence of sphingosine 1-phosphate lyase protein expression and activity downregulation in human neoplasm: implication for resistance to therapeutics in prostate cancer. *Mol Cancer Ther*. 2012;11(9):1841–1851.
69. White-Gilbertson S, et al. Ceramide synthase 6 modulates TRAIL sensitivity and nuclear translocation of active caspase-3 in colon cancer cells. *Oncogene*. 2009;28(8):1132–1141.
70. Mesicek J, et al. Ceramide synthases 2, 5, and 6 confer distinct roles in radiation-induced apoptosis in HeLa cells. *Cell Signal*. 2010;22(9):1300–1307.
71. Ardail D, et al. Diversity and complexity of ceramide generation after exposure of jurkat leukemia cells to irradiation. *Int J Radiat Oncol Biol Phys*. 2009; 73(4):1211–1218.
72. Merrill AH, van Echten G, Wang E, Sandhoff K. Fumonisin B1 inhibits sphingosine (sphinganine) N-acyltransferase and de novo sphingolipid biosynthesis in cultured neurons in situ. *J Biol Chem*. 1993;268(36):27299–27306.
73. Alphonse G, et al. p53-independent early and late apoptosis is mediated by ceramide after exposure of tumor cells to photon or carbon ion irradiation. *BMC Cancer*. 2013;13:151.
74. Wu WK, et al. The autophagic paradox in cancer therapy. *Oncogene*. 2012;31(8):939–953.
75. Apel A, Herr I, Schwarz H, Rodemann HP, Mayer A. Blocked autophagy sensitizes resistant carcinoma cells to radiation therapy. *Cancer Res*. 2008; 68(5):1485–1494.
76. Ferrer I, Barron S, Rodriquez-Farre E, Planas AM. Ionizing radiation-induced apoptosis is associated with c-Jun expression and c-Jun/AP-1 activation in the developing cerebellum of the rat. *Neurosci Lett*. 1995;202(1–2):105–108.
77. Lee YJ, et al. Effect of ionizing radiation on AP-1 binding activity and basic fibroblast growth factor gene expression in drug-sensitive human breast carcinoma MCF-7 and multidrug-resistant MCF-7/

ADR cells. *J Biol Chem*. 1995;270(48):28790–28796.
78. Jegga AG, Schneider L, Ouyang X, Zhang J. Systems biology of the autophagy-lysosomal pathway. *Autophagy*. 2011;7(5):477–489.
79. Pchejetski D, et al. FTY720 (fingolimod) sensitizes prostate cancer cells to radiotherapy by inhibition of sphingosine kinase-1. *Cancer Res*. 2010; 70(21):8651–8661.
80. Hannun YA, Obeid LM. Many ceramides. *J Biol Chem*. 2011;286(32):27855–27862.
81. Liu YY, et al. A role for ceramide in driving cancer cell resistance to doxorubicin. *FASEB J*. 2008; 22(7):2541–2551.
82. Kim WH, Kang KH, Kim MY, Choi KH. Induction of p53-independent p21 during ceramide-induced G1 arrest in human hepatocarcinoma cells. *Biochem Cell Biol*. 2000;78(2):127–135.
83. Alesse E, Zazzeroni F, Angelucci A, Giannini G, Di Marcotullio L, Gulino A. The growth arrest and downregulation of c-myc transcription induced by ceramide are related events dependent on p21 induction, Rb underphosphorylation and E2F sequestering. *Cell Death Differ*. 1998;5(5):381–389.
84. Komori H, Ichikawa S, Hirabayashi Y, Ito M. Regulation of UDP-glucose:ceramide glucosyltransferase-1 by ceramide. *FEBS Lett*. 2000;475(3):247–250.
85. Gamard CJ, Dbaibo GS, Liu B, Obeid LM, Hannun YA. Selective involvement of ceramide in cytokine-induced apoptosis. Ceramide inhibits phorbol ester activation of nuclear factor kappaB. *J Biol Chem*. 1997;272(26):16474–16481.
86. Ogretmen B, Kraveka JM, Schady D, Usta J, Hannun YA, Obeid LM. Molecular mechanisms of ceramide-mediated telomerase inhibition in the A549 human lung adenocarcinoma cell line. *J Biol Chem*. 2001;276(35):32506–32514.
87. Truman JP, et al. Down-regulation of ATM protein sensitizes human prostate cancer cells to radiation-induced apoptosis. *J Biol Chem*. 2005; 280(24):23262–23272.
88. Ogretmen B, et al. Biochemical mechanisms of the generation of endogenous long chain ceramide in response to exogenous short chain ceramide in the A549 human lung adenocarcinoma cell line. Role for endogenous ceramide in mediating the action of exogenous ceramide. *J Biol Chem*. 2002;277(15):12960–12969.
89. Mechta F, Lallemand D, Pfarr CM, Yaniv M. Transformation by ras modifies AP1 composition and activity. *Oncogene*. 1997;14(7):837–847.
90. Alani R, et al. The transactivating domain of the c-Jun proto-oncoprotein is required for cotransformation of rat embryo cells. *Mol Cell Biol*. 1991;11(12):6286–6295.
91. Johnson R, Spiegelman B, Hanahan D, Wisdom R. Cellular transformation and malignancy induced by ras require c-jun. *Mol Cell Biol*. 1996;16(8):4504–4511.
92. Schutte J, Minna JD, Birrer MJ. Deregulated expression of human c-jun transforms primary rat embryo cells in cooperation with an activated c-Ha-ras gene and transforms rat-1a cells as a single gene. *Proc Natl Acad Sci U S A*. 1989;86(7):2257–2261.
93. Zhang G, Dass CR, Sumithran E, Di Girolamo N, Sun LQ, Khachigian LM. Effect of deoxyribozymes targeting c-Jun on solid tumor growth and angiogenesis in rodents. *J Natl Cancer Inst*. 2004;96(9):683–696.
94. Bohmann D, Bos TJ, Admon A, Nishimura T, Vogt PK, Tjian R. Human proto-oncogene c-jun encodes a DNA binding protein with structural and functional properties of transcription factor AP-1. *Science*. 1987;238(4832):1386–1392.
95. Ludes-Meyers JH, Liu Y, Munoz-Medellin D, Hilsenbeck SG, Brown PH. AP-1 blockade inhibits the growth of normal and malignant breast cells. *Oncogene*. 2001;20(22):2771–2780.
96. Smith LM, Birrer MJ, Stampfer MR, Brown PH. Breast cancer cells have lower activating protein 1 transcription factor activity than normal mammary epithelial cells. *Cancer Res*. 1997;57(14):3046–3054.
97. O'Neill SM, Houck KL, Yun JK, Fox TE, Kester M. AP-1 binding transcriptionally regulates human neutral ceramidase. *Arch Biochem Biophys*. 2011;511(1–2):31–39.
98. Park JH, Eliyahu E, Narla G, DiFeo A, Martignetti JA, Schuchman EH. KLF6 is one transcription factor involved in regulating acid ceramidase gene expression. *Biochim Biophys Acta*. 2005;1732(1–3):82–87.
99. Halpern MT, Yabroff KR. Prevalence of outpatient cancer treatment in the United States: estimates from the Medical Panel Expenditures Survey (MEPS). *Cancer Invest*. 2008;26(6):647–651.
100. Delaney G, Jacob S, Featherstone C, Barton M. The role of radiotherapy in cancer treatment: estimating optimal utilization from a review of evidence-based clinical guidelines. *Cancer*. 2005;104(6):1129–1137.
101. Kim JJ, Tannock IF. Repopulation of cancer cells during therapy: an important cause of treatment failure. *Nat Rev Cancer*. 2005;5(7):516–525.
102. Beckham TH, et al. Acid ceramidase-mediated production of sphingosine 1-phosphate promotes prostate cancer invasion through upregulation of cathepsin B. *Int J Cancer*. 2012;131(9):2034–2043.
103. Narita M, et al. Spatial coupling of mTOR and autophagy augments secretory phenotypes. *Science*. 2011;332(6032):966–970.
104. Mohamed MM, Sloane BF. Cysteine cathepsins: multifunctional enzymes in cancer. *Nat Rev Cancer*. 2006;6(10):764–775.
105. Bernardo K, et al. Purification, characterization, and biosynthesis of human acid ceramidase. *J Biol Chem*. 1995;270(19):11098–11102.
106. Bai A, et al. Synthesis and bioevaluation of [omega]-N-amino analogs of B13. *Bioorg Med Chem*. 2009;17(5):1840–1848.
107. Thalmann GN, et al. Androgen-independent cancer progression and bone metastasis in the LNCaP model of human prostate cancer. *Cancer Res*. 1994; 54(10):2577–2581.
108. Wu HC, Hsieh JT, Gleave ME, Brown NM, Pathak S, Chung LW. Derivation of androgen-independent human LNCaP prostatic cancer cell sublines: role of bone stromal cells. *Int J Cancer*. 1994;57(3):406–412.
109. Zeidan YH, et al. Acid ceramidase but not acid sphingomyelinase is required for tumor necrosis factor-{alpha}-induced PGE2 production. *J Biol Chem*. 2006;281:24695–24703.
110. Xu R, Sun W, Jin J, Obeid LM, Mao C. Role of alkaline ceramidases in the generation of sphingosine and its phosphate in erythrocytes. *FASEB J*. 2010;24(7):2507–2515.
111. Fertil B, Dertinger H, Courdi A, Malaise EP. Mean inactivation dose: a useful concept for intercomparison of human cell survival curves. *Radiat Res*. 1984;99(1):73–84.